Journal of Fluids and Structures (1999) **13,** 3–35
Article No.: jfls.1998.0192
All articles available online at http://www.idealibrary.com on IDEAL

COMPARISON OF THEORY AND EXPERIMENT ON AEROACOUSTIC LOADS AND DEFLECTIONS

L. M. B. C. Campos†, A. Bourgine§ and B. Bonomi‡

†*Instituto Superior Técnico, 1096 Lisboa Codex, Portugal*
§*ONERA, 29 Ave. de la Division Leclerc, B.P. 72, Châtillon, 92322, France*
‡*Dassault Aviation, 78 Quai-Dassault, Saint-Cloud 92214, France*

(Received 11 June 1998 and in revised form 11 September 1998)

The correlation of acoustic pressure loads induced by a turbulent wake on a nearby structural panel is considered: this problem is relevant to the acoustic fatigue of aircraft, rocket and satellite structures. Both the correlation of acoustic pressure loads and the panel deflections, were measured in an 8-m diameter transonic wind tunnel. Using the measured correlation of acoustic pressures, as an input to a finite-element aeroelastic code, the panel response was reproduced. The latter was also satisfactorily reproduced, using again the aeroelastic code, with input given by a theoretical formula for the correlation of acoustic pressures; the derivation of this formula, and the semi-empirical parameters which appear in it, are included in this paper. The comparison of acoustic responses in aeroacoustic wind tunnels (AWT) and progressive wave tubes (PWT) shows that much work needs to be done to bridge that gap; this is important since the PWT is the standard test means, whereas the AWT is more representative of real flight conditions but also more demanding in resources. Since this may be the first instance of successful modelling of acoustic fatigue, it may be appropriate to list briefly the essential "positive" features and associated physical phenomena: (i) a standard aeroelastic structural code can predict acoustic fatigue, provided that the correlation of pressure loads be adequately specified; (ii) the correlation of pressure loads is determined by the interference of acoustic waves, which depends on the exact evaluation of multiple scattering integrals, involving the statistics of random phase shifts; (iii) for the relatively low frequencies (one to a few hundred Hz) of aeroacoustic fatigue, the main cause of random phase effects is scattering by irregular wakes, which are thin on wavelength scale, and appear as partially reflecting rough interfaces. It may also be appropriate to mention some of the "negative" features, to which may be attached illusory importance; (iv) deterministic flow features, even conspicuous or of large scale, such as convection, are not relevant to aeroacoustic fatigue, because they do not produce random phase shifts; (v) local turbulence, of scale much smaller than the wavelength of sound, cannot produce significant random phase shifts, and is also of little consequence to aeroacoustic fatigue; (vi) the precise location of sound sources can become of little consequence, after multiple scattering gives rise to a diffuse sound field; and (vii) there is not much ground for distinction between unsteady flow and sound waves, since at transonic speeds they are both associated with pressures fluctuating in time and space.

1. INTRODUCTION

The problem of acoustic fatigue occurs for structures exposed to sound of very high intensity (more than 150 dB, and as much as 170 dB); the corresponding acoustic pressure is sufficient to cause the vibration of structures, until cracks, either pre-existing or newly formed, grow, leading to eventual failure. Such high noise levels, well beyond the threshold of pain (110 dB) and damage (130 dB) to the human ear, occur for at least two kinds of aerospace vehicles: (i) near the exhaust of rocket engines of large space launchers, such as

0889–9746/99/010003 + 33 $30.00

the American Space Shuttle or European Ariane, where noise levels can exceed 170 dB, requiring certification of the entire vehicle, including the satellite payload, against acoustic fatigue; and (ii) the exhaust of jet engines of modern aircraft, as well as the turbulent wakes of control and high-lift surfaces, such as flaps, slats or spoilers, can also cause acoustic fatigue of nearby structures. Although acoustic fatigue is a major design issue for aerospace structures, the subject is almost wholly empirical, due to the lack of adequate models of acoustic pressure loads; the latter are random, and need to be specified as a spectrum correlated in space. The lack of prediction methods leads to acoustic fatigue design based on tests in progressive wave tubes (PWT), where noise levels up to about 155 dB can be generated; this is still a little too "low" for some applications. Another, more serious issue, is whether the distribution of acoustic pressure loads in a PWT, adequately represents the acoustic excitation of a structure in an AWT, e.g. in the vicinity a turbulent wake.

Among the aims of the project Acoufat (acoustic fatigue of composite and metal structures) was a careful investigation of the mechanisms of acoustic fatigue, to assess whether current testing techniques are reliable, and also if reasonably accurate prediction methods could be developed. It is not the aim of this paper to cover such a broad range of issues (Tougard *et al.* 1993, 1995), and in fact three related aspects are addressed: (i) experimental data obtained by the testing of a representative structural panel in a large high-subsonic wind tunnel, to measure both acoustic pressures and panel deformation; (ii) the prediction of the deformations, using a hybrid method, consisting of the finite-element aeroelastic code Elfini (Nicot & Petiau 1987) for the panel structure, using as input the spatial correlation of acoustic pressure spectra (or cross-spectra) measured in the wind tunnel; and (iii) a theoretical method, for the prediction of the deformation, using the same aeroelastic code, and cross-spectra specified by an analytical model, with semi-empirical parameters. The satisfactory agreement of the three sets of data must be rated as a step forward in the understanding of acoustic fatigue, beyond the empirical methods in current use, since: the agreement of (i) and (ii) shows that existing aeroelastic codes (such as Elfini) are capable of predicting acoustic response, provided that the correct spatial correlation of acoustic pressure spectra be fed in as an input (Section 2); the good agreement of (i) and (iii) is a first success at analytical modelling of acoustic fatigue (Section 3), since, although the analytical model involves semi-empirical parameters, the estimation or fitting of the latter, still represents some progress, relative to the totally empirical approach of the past.

At this stage it might be asked how well the acoustic response of the panel, in the aeroacoustic wind tunnel (AWT) correlates with the tests in PWTs; the correlation is unsatisfactory, as might be expected from the fact that acoustic excitation in an AWT may be different from that in a PWT, due to distinct effects of reflections from the walls and refraction by the mean flow. Since the eigenvalues and eigenfunctions of acoustic modes depend on the shape of the enclosure, acoustic fatigue tests in distinct PWTs can also give different results. It is not necessary to dwell any longer on acoustic fatigue testing in PWTs, since this lies beyond the scope of the present paper; the passing reference to PWTs, serves mainly to emphasize that a satisfactory representation of acoustic fatigue loads depends critically on adequate estimation of phase shifts, which specify the interference patterns of distinct wave components. Such interference patterns will be quite distinct for standing and propagating waves, and this is why one should not expect too much agreement between acoustic fatigue tests in PWTs and AWTs. The latter should be more representative of real flight conditions, and thus are the basis for a comparison of experiments and theory for aeroacoustic fatigue. The experiments (Section 3) show that the turbulent, recirculating flow behind a flap, can be quite complex both aerodynamically, and as a consequence, as concerns sources of sound; this is why the indication that phase correlations are the critical aspect is an important guide in the formulation of a theory (Section 2), which is sufficiently

simple to be analytically tractable, and yet stands some chance of success in comparison with the experiment. The theory is presented in Section 2, and the comparison with experiments in Section 3, with a brief concluding discussion in Section 4.

The aim of this paper is to model the correlation of random acoustic pressure loads on a panel, with relatively low frequencies around 100 Hz. The cause of the randomness cannot be the recirculating flow behind the flap, because it would lead to deterministic phase shifts. The turbulence contained in the recirculation bubble, or entrained in the wake of the flap, can cause phase shifts, but they would not be sufficiently significant, for a long wavelength, to cause significant interference between neighbouring wave components. Since the wavelength is larger than the scales of the flow, neither the mean flow nor the turbulent perturbations can be a significant cause for phase shifts. The wavelength is larger than the thickness of the shear layer (issuing from the flap), so that the latter appears as a randomly irregular interface. The sound waves radiated by or associated with the unsteady and turbulent flow behind the flap, are "trapped" between the wake and the structural panel. The word "associated" is used deliberately, because at high subsonic Mach numbers, unsteady flow is not distinguishable from sound. The word "trapped" is taken to mean that sound waves can have multiple reflections between the structural panel, taken as a rigid or compliant surface, and the turbulent shear layer, represented as a randomly irregular, partially reflecting interface. Thus, it is the reflections on the randomly irregular interface (and not the effects of recirculating flow or turbulent fluctuations), that cause random phase shifts, which specify the interference of neighbouring acoustic wave components, and thus the correlation of acoustic pressure loads on the structure, which in turn is the cause for fatigue. For an observation point close to the flap there is an edge effect, but this may not be dominant, because the interference of acoustic waves, and consequent randomness of the acoustic pressure loads, is mainly due to scattering between the structural panel and the turbulent wake. Also, an adequate representation of the correlation of acoustic pressure spectra is the essential element in the calculation of structural response, since the finite element code itself is already proven for other loads.

2. FORMULAS FOR THE SPATIAL CORRELATION OF TEMPORAL SPECTRA OF ACOUSTIC PRESSURES

The physical model (Figure 1), consists of the turbulent wake of a flap, generating sound waves, incident on a nearby structural panel, thereby causing acoustic fatigue. The sequence of calculations is as follows: in section 2.1 the pressure field is calculated for a plane wave component, taking into account multiple reflections between the structural panel and the turbulent wake, which, for low frequency sound of wavelength much larger than the thickness of the shear layer, appears as a randomly irregular interface; in Section 2.2 the multiple reflections of sound waves, by the irregular interface representing the turbulent wake, cause random phase shifts, which are used to calculate the space-time correlation of acoustic pressure; in Section 2.3 the statistics of the random phase shifts can be shown to be Gaussian (with zero mean), and thus are specified by the variance and correlation coefficient; in Section 2.4 the latter correlation coefficient for the phase (not to be confused with the correlation of pressure) has different forms for jets with and without volume conservation; the loads used as input for acoustic fatigue calculations are the temporal spectra of spatial correlation, and are calculated in Section 2.5 most simply at high frequencies, by asymptotic methods; the latter do not cover the whole frequency range, and thus an exact evaluation of spectra is performed in Section 2.6 involving Gaussian integrals in the nonvolume-conserving case; in the volume-conserving case, the spectra have Gaussian shape modified by Hermite polynomials (Section 2.7); if the observation point is close to the flap, the edge effect

introduces another modification to the spectra, specified by error functions (Section 2.8); the final formula, for the correlation normalized to the power spectrum, depends on eight parameters specifying the excitation source, correlation scales and scattering coefficients (Section 2.9).

2.1. Multiple Scattering Between a Shear Layer and a Wall

The sound field emitted by the turbulent wake may be decomposed into plane waves, and one component is considered, i.e.,

$$p_0(\mathbf{x}, z, t) = \mathrm{A}\exp\{\mathrm{i}(\mathbf{k}_0 \cdot \mathbf{x} + \gamma z - \omega_0 t)\}, \tag{1}$$

with horizontal wavevector $\mathbf{k}_0$, and vertical wavenumber given by

$$\gamma = |(\omega_0/c)^2 - k_0^2|^{1/2}, \qquad \omega_0 \equiv \omega_* - \mathbf{k}_0 \cdot \mathbf{U}, \tag{2a,b}$$

where c is the speed sound and ω_0 in (2b) is the Doppler-shifted frequency, i.e. the wave frequency ω_* modified by convection by the mean flow velocity $\mathbf{U}$. The reflection on the wall is specified (Rayleigh 1945; Brekhovskikh 1980) by a reflection factor R_+, and the reflection by the shear layer, represented as an interface with randomly irregular shape $z = \xi(\mathbf{x}, t)$, involves (Howe 1976; Campos 1978a) both amplitude R_- and phase ϕ changes:

$$p_1(\mathbf{x}, z, t) = R_+ R_- A \exp\{\mathrm{i}(\mathbf{k}_0 \cdot \mathbf{x} + \gamma z - \omega_0 t) + \mathrm{i}2\gamma\xi(\mathbf{x}, t), \tag{3}$$

i.e. the amplitude change is deterministic, and specified by the double reflection coefficient D,

$$D \equiv R_- R_+, \quad \phi(\mathbf{x}, t) = 2\gamma\xi(\mathbf{x}, t), \tag{4a,b}$$

whereas the phase change ϕ is random. The phase change is due to two effects (Campos 1997): (i) the Doppler shift due to turbulent velocity $\mathbf{u}(\mathbf{x}, t)$ superimposed on the mean flow velocity $\mathbf{U}$; and (ii) the phase shift due to the scattering of sound waves by the randomly irregular interface locally at height $z = \xi$ instead of at a fixed mean position. The latter effect is predominant at low frequencies, and thus is the only one included in equation (4b). In the case of n double reflections (Fig. 1) the acoustic pressure would be

$$p_n(\mathbf{x}, z, t) = D^n A \exp\left\{\mathrm{i}(\mathbf{k}_0 \cdot \mathbf{x} + \gamma z - \omega_0 t) + \mathrm{i}\sum_{m=1}^{n} \phi_m(\mathbf{x}, t)\right\}, \tag{5}$$

since the random phase shifts $\phi_1, \ldots, \phi_n$ may be different at each scattering event. Thus the total acoustic pressure is given, at the wall $z = 0$, by

$$p(\mathbf{x}, t) = \sum_{n=0}^{\infty} p_n(\mathbf{x}, t) = p_0(\mathbf{x}, t) \sum_{n=0}^{\infty} D^n \exp\left\{\mathrm{i}\sum_{m=1}^{n} \phi_m(\mathbf{x}, t)\right\}, \tag{6}$$

taking into account multiple scattering of all orders between the turbulent wake and the wall panel.

2.2. Correlation Function of Acoustic Pressure Loads

As usual in the theory of waves in random media (Uscinski 1977; Ishimaru 1978), including scattering by rough surfaces (Beckman & Spizzichino 1963; Ogilvy 1992), the correlation function of acoustic pressures is defined by

$$B(\mathbf{y}, \tau) \equiv \langle p(\mathbf{x} + \mathbf{y}, t + \tau) p^*(\mathbf{x}, t) \rangle, \tag{7}$$

where the asterisk denotes the complex conjugate, and $\langle \dots \rangle$ the statistical average; it is assumed that the statistical process is stationary, so that the correlation depends only on spatial $\mathbf{y}$ and temporal τ separation, but not on the events $(\mathbf{x}, t)$ and $(\mathbf{x} + \mathbf{y}, t + \tau)$ themselves. Substituting equation (6) in equation (7) yields

$$\mathrm{B}(\mathbf{y}, \tau) = \mathrm{p}_0(\mathbf{x} + \mathbf{y}, t + \tau)\, \mathrm{p}_0^*(\mathbf{x}, t) \sum_{n,m=0}^{\infty} D^{n+m} \langle \exp\{\mathrm{i}(\phi_1 + \cdots + \phi_n) - \mathrm{i}(\phi'_1 + \cdots + \phi'_m)\}\rangle, \tag{8}$$

denoting by $\phi_1, \dots, \phi_n$, the multiple phase shifts at $(\mathbf{x} + \mathbf{y}, t + \tau)$, and by $\phi'_1, \dots, \phi'_m$ the multiple phase shifts at $(\mathbf{x}, t)$. Normalizing the correlation function supresses a constant factor D^2,

$$D(\mathbf{y}, \tau) \equiv B(\mathbf{y}, \tau)/B(0, 0) = \exp\{\mathrm{i}(\mathbf{k}_0 \cdot \mathbf{y} - \omega_0 \tau))\, C(\mathbf{y}, \tau), \tag{9}$$

where C is the characteristic function,

$$C(\mathbf{y}, \tau) \equiv \sum_{n,m=1}^{\infty} D^{n+m-2} \langle \mathrm{Exp}\{\mathrm{i}(\phi_1 + \cdots + \phi_n - \phi'_1 - \cdots - \phi'_m)\}\rangle, \tag{10}$$

of a random process in $(n + m)$-variables, $(\phi_1, \dots, \phi_n; \phi_1, \dots, \phi'_m)$. Note that the effect of the mean flow velocity $\mathbf{U}$, appears in (2b), which is included in the deterministic phase term in (1) and hence in equation (9). The critical physical process determining the characteristic function (10) is the interference of acoustic waves, with random phase shift specified by relation (4b), due to the scattering by the irregular interface. It is this effect which will be analysed statistically next.

2.3. Characteristic Function of Random Phase Shifts

If the statistics of the process of acoustic scattering by the irregular shear layer are Gaussian (see below for justification), then the characteristic function depends only on the variances

$$\langle \{\phi_n(\mathbf{x} + \mathbf{y}, t + \tau)\}^2 \rangle = \sigma^2 = \langle \{\phi'_m(\mathbf{x}, t)\}^2 \rangle, \tag{11}$$

and correlation coefficients,

$$\mathrm{E}(\mathbf{x}, t) = \sigma^{-2} \langle \phi_n(\mathbf{x} + \mathbf{y}, t + \tau) \phi_m(\mathbf{x}, t) \rangle, \tag{12}$$

of the random phases, which are assumed to be all equal, i.e. independent of n and m. Then the characteristic function

$$C(\mathbf{y}, \tau) \equiv \exp\{ -[a - b\, \mathrm{E}(\mathbf{y}, \tau)]\}, \tag{13}$$

depends (von Mises 1964) on the total variance a of the (n + m) random variables,

$$2a = (n + m)\sigma^2, \quad 2b = [2nm + n(n - 1) + m(m - 1)]\sigma^2, \tag{14a,b}$$

and on the total correlation b (Campos 1992). Thus, the characteristic function is given by

$$C(\mathbf{y}, \tau) = \sum_{n,m=1}^{\infty} D^{n+m-2} \exp\{ -\sigma^2 [(n + m)/2 - (n + m)(n + m - 1)\mathrm{E}(\mathbf{y}, \tau)]\}, \tag{15}$$

under the assumption of a Gaussian process. The assumption of Gaussian statistics agrees with observations of sound transmission through turbulent wakes (Schmidt & Tillman 1970); it can also be justified (Campos 1978a) as follows: (i) since the correlation of random

phase shifts (12) tends to zero $\mathrm{E} \to 0$ for large separation $t \to \infty$, the Ergodic Theorem (Khinchin 1948) implies that averages over time … and over events $\langle \ldots \rangle$ are equal; (ii) since scattering of sound by the shear layer depends on the random shape of the latter $z = \xi(\mathbf{x}, t)$, events sufficiently separated are statistically independent as required by the Central Limit Theorem; and (iii) the latter applies, since the Lindeberg (1922) condition, requiring that widely separated events have negligible effect on the variance, is met (Campos 1984, 1986). Note that all these statistical effects depend on the scattering of sound by the randomly irregular shape of the interface representing the turbulent wale of the flap (Figure 1), and not on the convection of acoustic waves by the mean flow, which appears as a deterministic phase term in equation (9).

2.4. Distinction Between Jets with and without Volume Conservation

To complete the statistical description of the sound field it is necessary to specify the correlation (12) of random phase shifts, which depends on equation (4b), the correlation of the randomly irregular shape of the shear layer

$$\mathrm{E}(\mathbf{y}, \tau) = (2\gamma/\sigma)^2 \langle \xi(\mathbf{x} + \mathbf{y}, t + \tau) \xi(\mathbf{x}, t) \rangle; \tag{16}$$

it has already been assumed in equation (7), and hence also in equations (15) and (16), that the scattering process is stationary, i.e. depends only on spatial $\mathbf{y}$ and temporal τ separation, and not on the events $(\mathbf{x}, t)$. A further assumption is the statistical independence in space–time for the correlation of phase shifts

$$\mathrm{E}(\mathbf{y}, \tau) = \mathrm{E}(x/L)\, \mathrm{E}(y/\ell)\, \mathrm{E}(\tau/T), \tag{17}$$

where T is the correlation time, and L and ℓ are the longitudinal and transverse correlation lengths. Statistical independence in space–time for the characteristic function (15), instead of equation (17), would lead to distinct spectra (Campos 1997). A typical correlation function

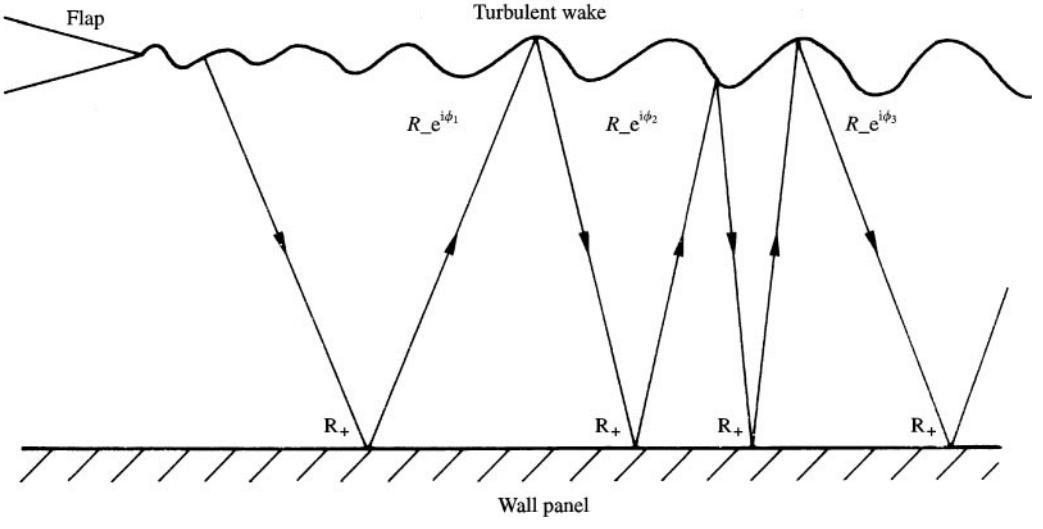

Figure 1. Multiple scattering of sound between a wall structural panel and a turbulent shear layer trailing from a flap, showing the deterministic reflection coefficients $R_{\pm}$ which are equal at each reflection, and random phase shifts $\phi_1, \phi_2, \phi_3, \ldots$ which are generally different for each event.

(Campos 1996) is small $E \ll 1$ for events spaced more than a correlation length $x \gg L$, e.g. is given by a Gaussian

$$E(x/L) = (1 + gx^2/L^2)e^{-x^2/L^2}, \tag{18}$$

multiplied by a polynomial, for which the simplest symmetric quadratic form is taken. The integral is given by

$$\int_{-\infty}^{+\infty} E(x/L)dx = L\sqrt{\pi}(1 + g/2) \tag{19}$$

for the family of correlation coefficients (18), with parameter g.

In order for the volume of the fluid between the wall and the shear layer to be conserved (within a correlation length)

$$\int_{-\infty}^{+\infty} \xi(\mathbf{x}, t)\,dx = 0 \Rightarrow \int_{-\infty}^{+\infty} E(x/L)\,dx = 0, \tag{20}$$

the integral (19) should vanish when $g = -2$, i.e. this leads to the correlation coefficient (Campos 1978b)

$$g = -2: \quad E_1(x/L) = (1 - 2x^2/L^2)e^{-x^2/L^2}, \tag{21}$$

which is negative $E_1 < 0$ for large separations $x > L/\sqrt{2}$, because in order for the integral (20) to vanish, the displacements ξ must have reversed signs at some distance x. The simpler purely Gaussian correlation coefficient

$$g = 0; \qquad E_0(x/L) = e^{-x^2/L^2}, \tag{22}$$

would not, by (19), be volume conserving, see (20). The negative correlations (21) have been observed (Ho & Kovasznay 1976a, b) for sound transmitted through turbulent jets. This is illustrated in Figure 2, which shows the two cases: (a) for an expanding (contracting) jet, the displacements ξ, ξ' from the mean position are of the same sign, i.e. both positive $\xi, \xi' > 0$ (negative $\xi', \xi < 0$), and hence their product $\xi'\,\xi$ is positive, leading to a positive correlation, like equation (22); (b) for a volume-conserving jet, a positive displacement $\xi > 0$ must give way to a negative one $\xi' < 0$ at some separation, so that the product is negative, $\xi'\,\xi < 0$, as for the correlation (21) for $x > L/\sqrt{2}$.

2.5. Asymptotic and Exact evaluation of Power Spectra

The load input to structural calculations is the temporal spectrum of the correlation of acoustic pressures (9):

$$F(\mathbf{x}; \omega) = \int_{-\infty}^{+\infty} D(\mathbf{x}, t)\,e^{i\omega t}\,dt, \tag{23}$$

which depends on the characteristic function

$$F(\mathbf{x}; \omega) = e^{i\mathbf{k}_0 \cdot \mathbf{x}} \int_{-\infty}^{+\infty} e^{i(\omega - \omega_0)t}\,C(\mathbf{x}, t)\,dt, \tag{24}$$

i.e. involves by equations (13) and (17) generalized Gaussian integrals

$$F(\mathbf{x}, \omega) = e^{ik_0 \cdot x} \sum_{n,m=1}^{\infty} D^{n+m-2} \int_{-\infty}^{+\infty} \exp\{i(\omega - \omega_0)t - a + b\,E(x/L)E(y/\ell)E(t/T)\}\,dt. \tag{25}$$

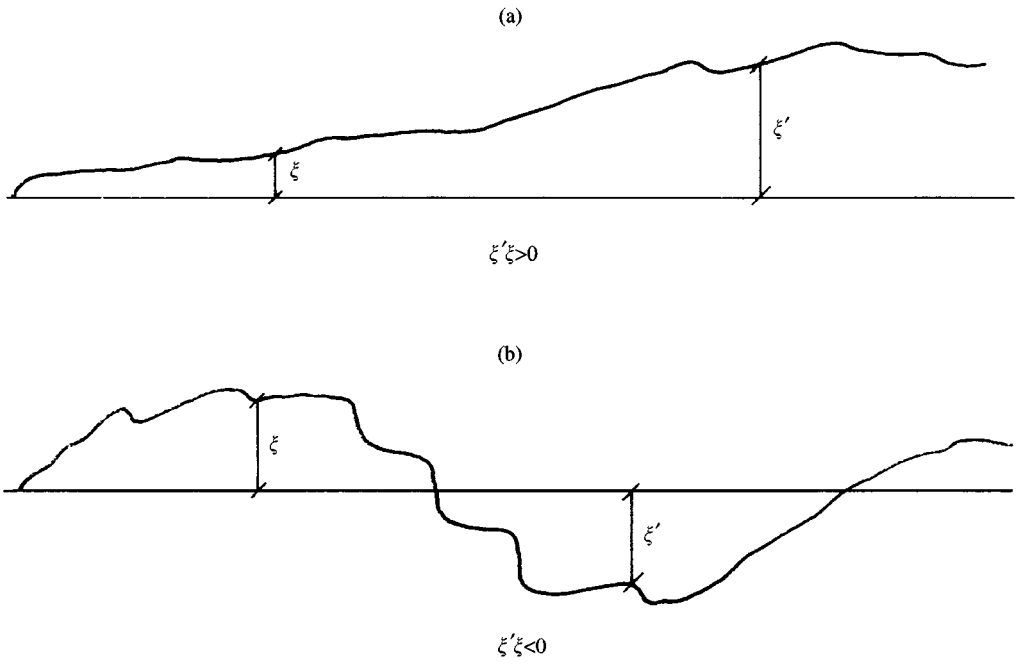

Figure 2. The correlation of displacements, and hence of acoustic phase shifts, are (a) always positive for an expanding jet, whereas (b) for a volume-conserving jet they must be negative for some separations.

If all random scattering effects are neglected $\sigma = 0$, i.e. $a = 0 = b$ in equation (14a,b), the integral (25) is evaluated as a Dirac delta function

$$F(\mathbf{x}; \omega) = \exp(\mathrm{i}\mathbf{k}_0 \cdot \mathbf{x})\, 2\pi\delta(\omega - \omega_0)[D(1 - D)]^{-2}, \tag{26}$$

showing that the spectrum is a spike at excitation frequency $\omega = \omega_0$, eventually with a Doppler shift (2b) due to the mean flow. Taking the autocorrelation of acoustic pressure, or power spectrum

$$G(\omega) \equiv F(0; \omega) = \int_{-\infty}^{+\infty} \exp\{\mathrm{i}(\omega - \omega_0)t - a + b\,\mathrm{E}(t/T)\}\,\mathrm{d}t, \tag{27}$$

for one term of the series (the others are treated similarly), in the case of strong random effects, i.e. large σ^2, a, and b, the integral can be evaluated asymptotically (Campos 1978b) by the method of stationary phase, using the lowest orders in the power series expansion of

$$\alpha \equiv 1 - g: \quad -a + b\,E(t/T) = -a + b - b\alpha t^2/T^2 + 0(t^4/T^4), \tag{28}$$

where $\alpha = 1 - g$ for equation (18), and hence $\alpha = 1$ for equation (22), and $\alpha = 3$ for equation (21). The spectrum at high frequency,

$$G(\omega) \sim \int_{-\infty}^{+\infty} \exp\{\mathrm{i}(\omega - \omega_0)t - a + b - b\alpha t^2/T^2\}\,\mathrm{d}t = \mathrm{e}^{b-a}\,T\sqrt{\pi/b\alpha}$$
$$\times \exp\{-(\omega - \omega_0)^2\,T^2/4b\alpha\}, \tag{29}$$

has a Gaussian shape, with peak at the excitation frequency $\omega = \omega_0$, and is broader for shorter correlation time T and larger total variance b.

2.6. Evaluation Spectra of Using Generalized Gaussian Integrals

The asymptotic approximation $(\omega - \omega_0)\, T/2\sqrt{b\alpha}$ large, is not valid for the whole frequency range of interest in experiments; in particular, it fails for frequencies ω close to the excitation frequency ω_0, which is the most important part of the spectrum. Thus, the exact spectrum is needed, at all frequencies, and is specified via (27) by

$$G(\omega) = \mathrm{e}^{-a}\left\{\int_{-\infty}^{+\infty} \mathrm{e}^{\mathrm{i}(\omega-\omega_0)t}\,\mathrm{d}t + \sum_{n=1}^{\infty}\frac{b^n}{n!}\int_{-\infty}^{+\infty}\{\mathrm{E}(t/T)\}^n \mathrm{e}^{\mathrm{i}(\omega-\omega_0)t}\,\mathrm{d}\omega\right\}, \tag{30}$$

and depends on the form of the correlation coefficient E. For tests of a structural specimen in a pressure wave tube the nonvolume-conserving form (22) may be appropriate, viz,

$$G(\omega) = \mathrm{e}^{-a}\left\{2\pi\delta(\omega-\omega_0) + \sum_{n=1}^{\infty}\frac{b^n}{n!}\int_{-\infty}^{+\infty}\mathrm{e}^{\mathrm{i}(\omega-\omega_0)t - nt^2/T^2}\,\mathrm{d}t\right\}, \tag{31}$$

so that the spectrum consists of an attenuated spike ($\mathrm{e}^{-a} < 1$) at excitation frequency $\omega = \omega_0$:

$$G(\omega) = \mathrm{e}^{-a}\left\{2\pi\,\delta(\omega-\omega_0) + T\sqrt{\pi}\sum_{n=1}^{\infty}\frac{b^n}{n!\sqrt{n}}\int_{-\infty}^{+\infty}\exp\{-(\omega-\omega_0)^2\,T^2/4n\}\right\}, \tag{32}$$

plus a sequence of Gaussian bands, broader as n increases. Note that, so far, only standard Gaussian integrals,

$$I_0 \equiv \int_{-\infty}^{+\infty}\mathrm{e}^{\mathrm{i}\beta t - \alpha t^2}\,\mathrm{d}t = \sqrt{\pi/\alpha}\,\mathrm{e}^{-\beta^2/4\alpha}, \tag{33}$$

have been used in the evaluation of spectra, viz., equations (29) and (31), (32), but in the sequel, generalizations of equation (33) will be needed.

2.7. Modification of Spectra by Hermite Polynomials

In the case of tests with a structural specimen in an aerodynamic wind tunnel, the volume conserving correlation coefficient (21) should be used in equation (30):

$$G(\omega) = \mathrm{e}^{-a}\left\{\int_{-\infty}^{+\infty}\mathrm{e}^{\mathrm{i}(\omega-\omega_0)}\,\mathrm{d}t + \sum_{n=1}^{\infty}(b^n/n!)\int_{-\infty}^{+\infty}\mathrm{e}^{\mathrm{i}(\omega-\omega_0)t - nt^2/T^2}(1-2t^2/T^2)^n\,\mathrm{d}t\right\} \tag{34}$$

leading to

$$G(\omega) = \mathrm{e}^{-a}\left\{2\pi\,\delta(\omega-\omega_0) + \sum_{n=1}^{\infty}(b^n/n!)\sum_{p=0}^{n}\binom{n}{p}(-2/T^2)^p\int_{-\infty}^{+\infty}t^{2p}\,\mathrm{e}^{\mathrm{i}(\omega-\omega_0)t - nt^2/T^2}\,\mathrm{d}t\right\} \tag{35}$$

where $\binom{n}{p} \equiv n!/[p!\,(m-p)!]$. Expression (35) involves generalized Gaussian integrals

$$I_{2p} \equiv \int_{-\infty}^{+\infty} t^{2p}\,\mathrm{e}^{\mathrm{i}\beta t - \alpha t^2}\,\mathrm{d}t = (-)^p\,d^{2p}I_0/d\beta^{2p}, \tag{36}$$

which can be evaluated by differentiation of equation (33); since the derivatives of a Gaussian specify Hermite polynomials (Courant & Hilbert 1953; Campos 1989):

$$\mathrm{H}_m(\vartheta) \equiv (-)^m\,\mathrm{e}^{\vartheta^2}\,d^m(\mathrm{e}^{-\vartheta^2})/\mathrm{d}\vartheta^m, \tag{37}$$

the generalized Gaussian integral (36) is evaluated from equations (33) and (37) as

$$\int_{-\infty}^{+\infty} t^{2p} \mathrm{e}^{\mathrm{i}\beta t - \alpha t^2} \mathrm{d}t = 2^{-2p}(-)^p \sqrt{\pi}\alpha^{-p-1/2} \mathrm{e}^{-\beta^2/4\alpha} \mathrm{H}_{2p}(\beta/2\sqrt{\alpha}), \tag{38}$$

which simplifies to equation (33) for $p = 0$. Using this result equation (38) in equation (35) leads to the spectrum

$$G(\omega) = \mathrm{e}^{-a} \left\{ 2\pi\, \delta(\omega - \omega_0) + T\sqrt{\pi} \sum_{n=1}^{\infty} (b^n/\sqrt{n}) \mathrm{e}^{-\eta^2} \sum_{p=0}^{n} [(8n)^{-p}/p!(n-p)!]\, \mathrm{H}_{2p}(\eta) \right\}, \tag{39a}$$

$$\eta \equiv (\omega - \omega_0) T/2\sqrt{n}, \tag{39b}$$

where the shapes of the Gaussian bands are modified by Hermite polynomials. Returning to the correlation function of acoustic pressure (25), the evaluation is similar to that leading from equation (27) to (39a,b), provided that the substitution

$$b \to b\, \mathrm{E}(x/L)\, E(y/\ell) \Rightarrow G(\omega) \to F(x, y; \omega) \tag{40a}$$

is made, leading to

$$F(x, y; \omega) = \mathrm{e}^{-a} \left\{ 2\pi\, \delta(\omega - \omega_0) + T\sqrt{\pi} \sum_{n=1}^{\infty} (b^n/\sqrt{n}) [\mathrm{E}(x/L)\mathrm{E}(y/\ell)]^n \right.$$
$$\left. \sum_{p=0}^{n} [(8n)^{-p}/p!(n-p)!] \mathrm{e}^{-\eta^2} \mathrm{H}_{2p}(\eta) \right\}, \tag{40b}$$

where only the temporal spectrum (but not spatial spectra) was taken.

2.8. Edge Effect for Flap of Finite Span and Error Functions

It is possible in addition, to take the spatial spectrum, which is given by

$$H(k, K, \omega) = \int_{-\infty}^{x} \mathrm{d}x \int_{-B-Y}^{B-Y} \mathrm{d}y\, \mathrm{e}^{-\mathrm{i}(kx + Ky)} F(x, y; \omega), \tag{41}$$

where (Figure 3) in the vicinity of a flap, for an observer position (X, Y), (i) the edge effect is accounted for by integrating over $-X < x < +\infty$, and (ii) the effect of the finite span 2B is taken into account by integrating over $-B - Y < y < B - Y$. This approximate account of diffraction effects may be sufficient, because the main contribution to the spectrum comes from multiple scattering between the wall panel and the irregular wake. Substituting equation (40b) into equation (41) leads to integrals of type

$$\int_{-X}^{\infty} (1 - 2x^2/L^2)^n \mathrm{e}^{-nx^2/L^2 - \mathrm{i}(k - k_0)x} \mathrm{d}x = \sum_{p=0}^{n} \binom{n}{p} (-2/L^2)^p \int_{-\infty}^{X} x^{2p} \mathrm{e}^{-nx^2/L^2 + \mathrm{i}(k - k_0)x} \mathrm{d}x, \tag{42}$$

which are reducible to the generalized Gaussian type

$$I_{2p}(X) \equiv \int_{-\infty}^{X} x^{2p} \mathrm{e}^{\mathrm{i}\beta x - \alpha x^2} \mathrm{d}x = (-)^{\mathrm{P}} \mathrm{d}^{2p} \{I_0(X)\}/\mathrm{d}\beta^{2p}, \tag{43}$$

where

$$I_0(X) = \sqrt{\pi/\alpha}\, \mathrm{e}^{-\beta^2/4\alpha} \{1 + \mathrm{erf}(X\sqrt{\alpha} - \mathrm{i}\beta/2\sqrt{\alpha})\}/2 \tag{44}$$

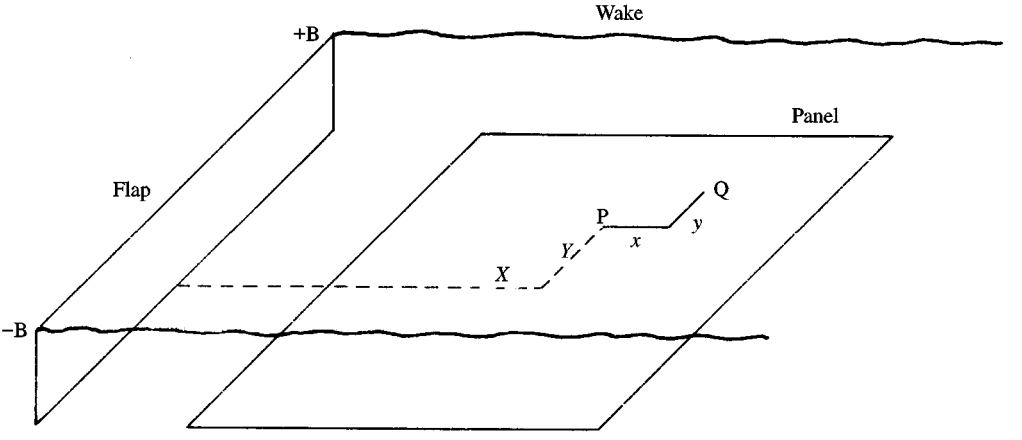

Figure 3. Position $P \equiv (X, Y)$ of observer relative to the wake of flap for measurement of spectra, and correlations between positions $P \equiv (X, Y)$ and $Q \equiv (X + x, Y + y)$.

involves error functions (Abramowitz & Stegun 1965)

$$\operatorname{erf}(\vartheta) \equiv (2/\sqrt{\pi}) \int_0^{\vartheta} \mathrm{e}^{-\eta^2}\, \mathrm{d}\eta. \tag{45}$$

Substituting equation (44) into (43), using Leibnitz's rule for the product of derivatives, and also differentiation formulas for Gaussian (37) and error (45) functions, yields

$$I_{2p}(X) = \int_{-\infty}^{X} x^{2p} \mathrm{e}^{\mathrm{i}\beta x - \alpha x^2}\, \mathrm{d}x = 2^{-2p}(-)^p \alpha^{-p-1/2}\, \mathrm{e}^{-\vartheta^2} \{\sqrt{\pi}\, \mathrm{H}_{2p}(\vartheta)[1 + \exp(\zeta)]/2$$
$$- \sum_{q=1}^{2p} q[(-\mathrm{i})^{q-1}(2p)!/q!(2p-q)!\, \mathrm{H}_{2p-q}(\vartheta) \mathrm{e}^{-\zeta^2}\, \mathrm{H}_{q-1}(\zeta)\}, \tag{46a}$$

where

$$\vartheta \equiv \beta/2\sqrt{\alpha}, \quad \zeta \equiv X\sqrt{\alpha} - \mathrm{i}\vartheta. \tag{46b,c}$$

Thus the exact spectrum, with edge and finite span effects (41) and (42) can be evaluated using, (46a)–(46c).

2.9. Excitation, Correlation and Scattering Parameters

In the preceding exposition a number of distinct spectra has been obtained, viz., with edge effect and flap of finite span (Section 2.8), or for an infinite irregular shear layer, either volume conserving (Section 2.7) or not (Section 2.6). In the case of single scattering, $D = 0$, there is a single integral in (25), with $n = 1 = m$ in equation (14a,b), viz., $a = \sigma^2 = b$. In the case of multiple scattering $D \neq 0$, there is a series of integrals, i.e. equation (25) and (40b), which specify the correlation of the acoustic pressure spectra at relative positions (x, y):

$$F(x, y; \Omega) = \exp\{\mathrm{i}(k_0 x + K_0 y)\} \sum_{n,m=1}^{\infty} D^{n+m-2}\, \mathrm{e}^{-a}$$
$$\times \left\{ 2\pi\delta(\Omega) + \sum_{j=1}^{\infty} (b^j/\sqrt{j})[(1 - x^2/2L^2)(1 - y^2/2\ell^2)]^j \right.$$
$$\left. \times \exp\{-j[(x/L)^2 + (y/\ell)^2]\} \exp(-\Omega^2/4j) \sum_{p=0}^{j} [(8j)^{-p}/p!(j-p!)]\, \mathrm{H}_{2p}(\Omega/2\sqrt{j}), \right. \tag{47}$$

where $\Omega \equiv (\omega - \omega_0)T$ is the dimensionless frequency. The correlation may be normalized to the power spectrum

$$H(x, y; \Omega) \equiv F(x, y; \Omega)/G(\Omega), \quad G((\omega - \omega_0)T) \equiv G(\Omega) \equiv G(\omega)/T, \tag{48a,b}$$

where, from equation (39a,b),

$$G(\Omega) = \sum_{n,m=1}^{\infty} D^{n+m-2} \mathrm{e}^{-a} \left\{ 2\pi\, \delta(\Omega) + \sum_{j=1}^{\infty} (b^j/\sqrt{j}) \exp(-\Omega^2/4j) \right.$$
$$\left. \times \sum_{p=0}^{j} [(8j)^{-p}/p!(j-p)!\, \mathrm{H}_{2p}(\Omega/2\sqrt{j}) \right\}. \tag{49}$$

The formulas depend on eight parameters: (i) the frequency ω_0, longitudinal k_0 and transverse K_0 wavenumbers of excitation; (ii) the correlation time T, and length, both longitudinal L and transverse ℓ; (iii) the r.m.s. phase shift σ; and (iv) the double reflection coefficient D. The variables are the relative position (x, y) and frequency ω, all of which appear in dimensionless form x/L, y/ℓ, $(\omega - \omega_0)T$.

3. PANEL DEFORMATIONS AND ACOUSTIC PRESSURES MEASURED IN A WIND TUNNEL

In order to proceed to the comparison of theory with experiment, the following aspects have to be addressed: in Section 3.1 the correlation of acoustic pressures is used as an input, to the finite element code Elfini (of Dassault Aviation), which calculates panel displacements; the installation of the panel, instrumented with strain gauges to measure strains, and microphones to measure sound pressures, in the Modane S1 wind tunnel is discussed in Section 3.2; the relevant flow conditions are analysed in Section 3.3, e.g. the recirculation bubble, behind the flap located upstream of the panel, and used to generate the turbulent wake, is not really important, but the irregular shape of the wake is; the distribution of sensors on two panels, one fitted with strain gauges and the other with microphones is presented in Section 3.4; the power spectra of sound measured at several of the 40 microphone positions are presented in Section 3.5; the cross-correlation of acoustic pressures at some pairs from the many possible combinations $\binom{40}{2} = 780$ of two microphones are discussed in Section 3.6; in Section 3.7 the comparison is made of panel response (a) measured by strain gauges, with the calculation of the Elfini code, (b) using a correlation of acoustic pressures measured by microphones, or (c) specified by the theory; in Section 3.8 the measured (b) correlation of acoustic pressures is compared with the theory (c) to fit the semi-empirical parameters in the latter; in Section 3.9 the importance of the correlation of loads is further highlighted by comparisons between fatigue tests, of the same panel, in the wind tunnel and in progressive wave tubes.

3.1. Acoustic Response of a Structural Panel

A typical aircraft structural panel, of multi-bay construction, is illustrated in Figure 4. Since it is symmetric, only one-half need be modelled by finite elements (Figure 5): a finer mesh is used in the central cell, since in this region the deformations may be greatest. The method of calculation of response is illustrated schematically in Figure 6 in two cases: (top) using a fine mesh, in the case of deterministic excitation, e.g. modelling of shaker tests; (bottom) using a coarser mesh, for random loads, together with a correlation function between elements, e.g. in the modelling of acoustic fatigue. The finite element discretization represents the

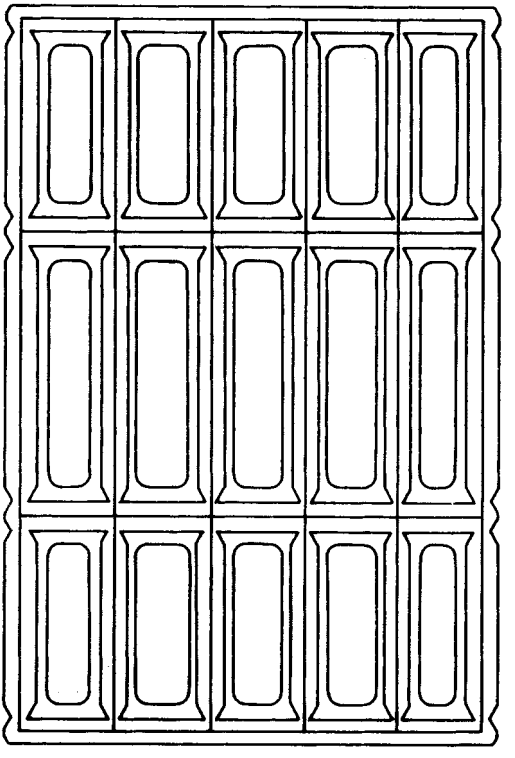

Figure 4. Typical aircraft aluminium structural panel of multi-bay construction.

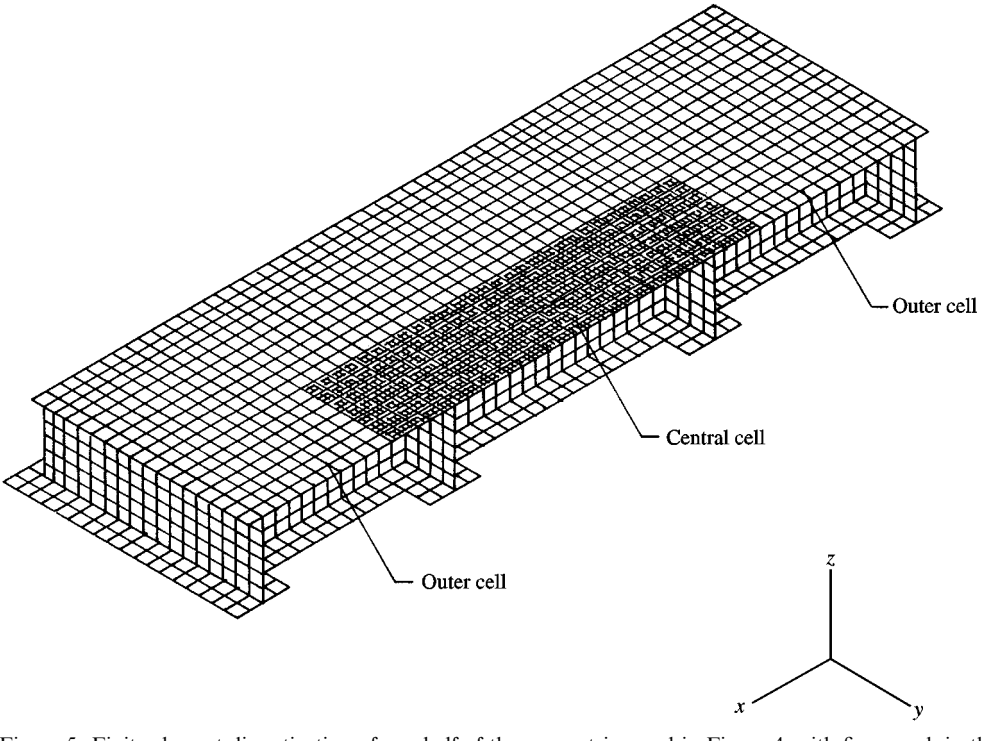

Figure 5. Finite-element discretization of one-half of the symmetric panel in Figure 4, with finer mesh in the central bay, where oscillation amplitudes may be larger.

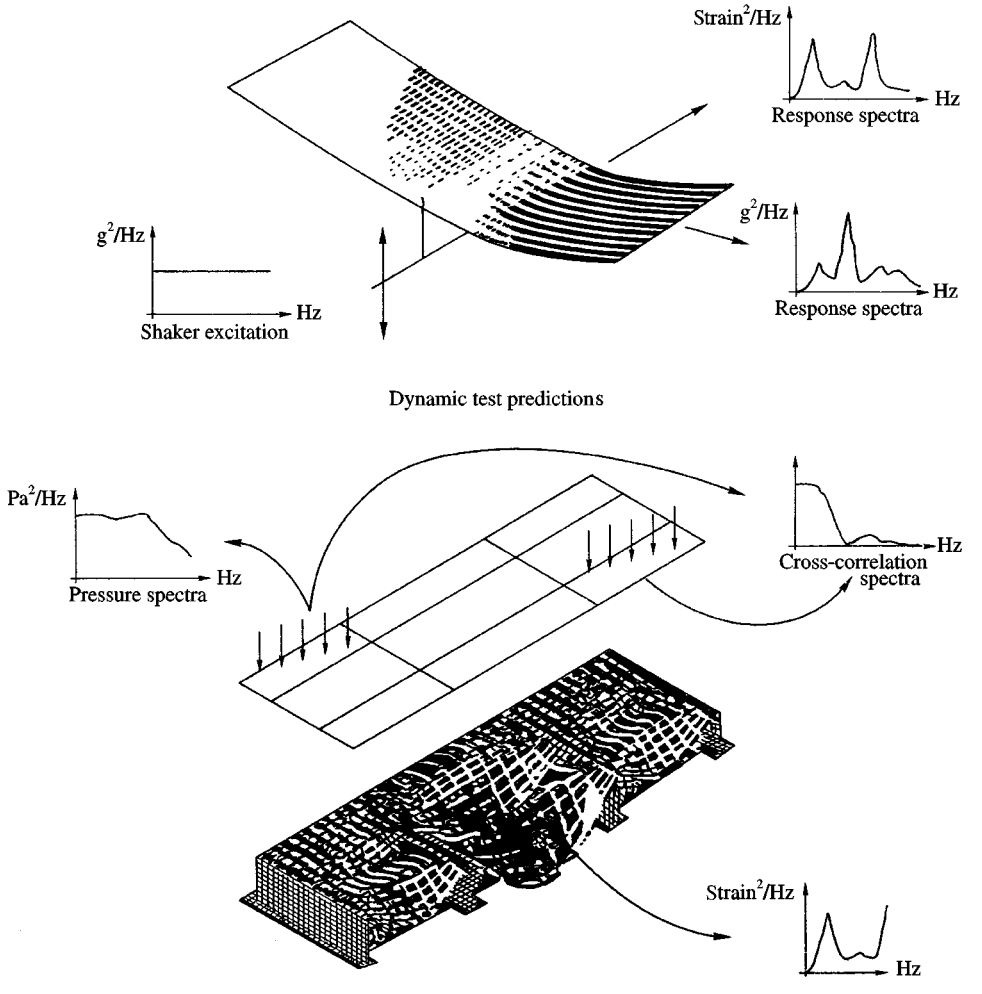

Figure 6. Prediction of panel response using (top) a fine mesh for deterministic loads as those due to shaker excitation, and (bottom) a coarse grid for correlation of loads in the random loads case, of interest to acoustic fatigue.

panel by a system of second-order, linear, coupled differential equations for the displacement Z_n:

$$n, m = 1, \ldots, N: \qquad A_{mn}\ddot{Z}_n + B_{mn}\dot{Z}_n + C_{mn}Z_n = Q_m(t), \tag{50}$$

where A_{mn}, B_{mn}, C_{mn} are mass, damping and stiffness matrices, and $Q_m(t)$ the forcing load. In the absence of the latter, the natural modes have frequencies ω_n and dampings λ_n, specified by the roots of

$$\zeta \equiv \omega + \mathrm{i}\lambda: \qquad \mathrm{Det}(-A_{mn}\zeta^2 + \mathrm{i}B_{mn}\zeta + C_{mn}) = 0. \tag{51}$$

The inverse $D_{\ell m}$ of the same matrix satisfies

$$\delta_{\ell n} = \sum_m D_{\ell m}(-A_{mn}\zeta^2 + \mathrm{i}B_{mn}\zeta + C_{mn}), \tag{52}$$

where $\delta_{\ell n}$ is the identity or unit matrix (or Kronecker delta), specifies the nonresonant response to a load of spectrum $\tilde{Q}(\omega)$:

$$\tilde{Z}_n(\omega) = \sum_m D_{nm}(\omega + \mathrm{i}\,\lambda)\tilde{Q}_m(\omega), \tag{53}$$

where a tilde denotes the Fourier transform. The correlation of loads at two points,

$$\langle \tilde{Z}_n \tilde{Z}_r \rangle = \sum_{m,s} D_{nm} D_{rs} \langle \tilde{Q}_m \tilde{Q}_s \rangle, \tag{54}$$

specifies the correlation of displacements. Some mode shapes are illustrated in Figures 7 and 8, respectively with symmetric and skew-symmetric boundary conditions. Concerning the symmetric modes in Figure 7, the fundamental s = 1 shows greater deflections in the central region, which is also the case for some harmonics s = 5, 15. There are modes with larger deflections away from the central region s = 4, 11, and modes for which the vibrations are noticeable over most of the panel s = 12. Concerning the skew-symmetric modes in Figure 8, there are also examples with deflections mostly in the central region a = 1, in peripheral regions a = 3, 11 and distributed over most of the panel a = 7, 8, 14. In the case of interest, the excitation of the modes is due to loads of aeroacoustic origin.

3.2. Set-up in an 8-Meter Transsonic Wind Tunnel

The most realistic simulation of aeroacoustic loads, except for real flight conditions, is provided by a wind tunnel; the facility used was one of the largest in Europe, the Modane S1 transonic wind tunnel, which has a circular cross-section with 8-m diameter. The photograph in Figure 9, and the sketch in Figure 10, show the arrangement: (i) a flap is used to generate a turbulent wake; (ii) behind the flap there is a flat surface, where the test panel lies flush; (iii) the whole assembly is mounted in a box, supported on the tunnel wall by means of struts. The design takes into consideration the following points: (i) the flap is interchangeable, with choice of three heights and two widths; (ii) the ensemble is set at some distance from the tunnel wall, so as to avoid the boundary layer, and to lie in the "potential core" of the test-section; (iii) the small frontal area minimizes the "blockage" of the wind tunnel, which can lead to unsteady measurement conditions and limit the Mach number achievable in the test-section. The set-up is not representative of typical aircraft situations, in one respect, which represents a deliberate simplification, to allow a clearer interpretation of results. In a real aircraft flap, slat, or spoiler, there is a gap between the moveable surface and the wing; this additional effect was omitted here, by mounting the flap onto the structure. Two different panels were successively mounted on the test-bed, downstream the flaps, during the AWT tests, in view of measuring, with the same external parameters of the mean flow, the following:

(i) the aeroacoustic fluctuating pressures at the wall, with appropriate sensors (microphones), acting as pressure transducers; this first panel was very thick (10 mm), clamped on its edges, so as to avoid or to minimize vibrations or aeroelastic interactions in the frequency range of interest (rigid wall approximation), thus measuring the incident acoustic field;

(ii) the induced vibrational field experienced by the second "panel" (the upper face of a structural box representative of typical aircraft structures), due to the same statistical distribution of external random loads;

(iii) together, aeroelastic coupling with the external flow and forced motion due to the fluctuating pressures can be involved in the structural response of the box; then, both of

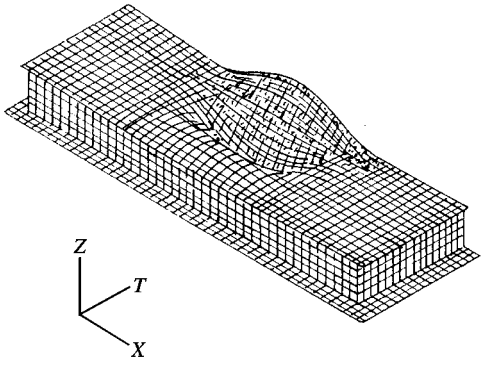

s = 1

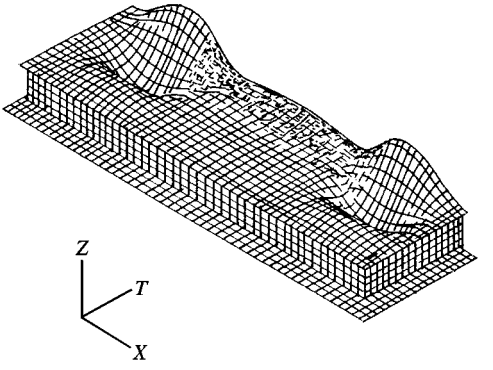

s = 4

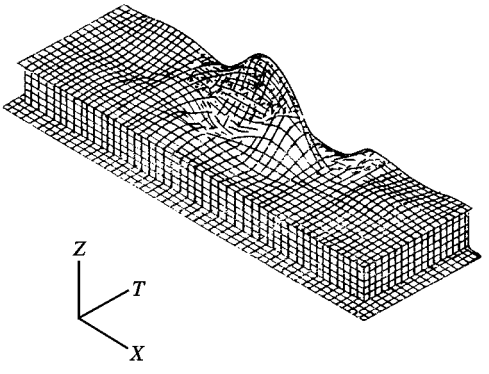

s = 5

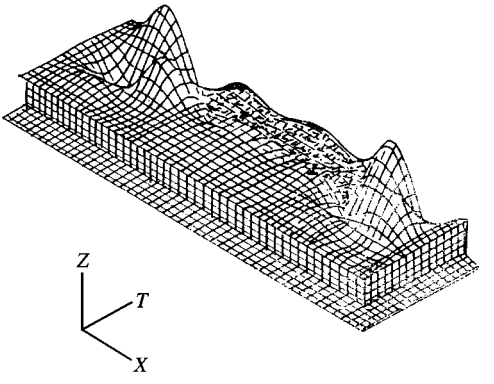

s = 11

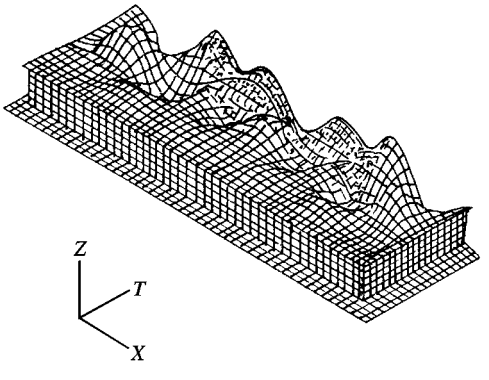

s = 12

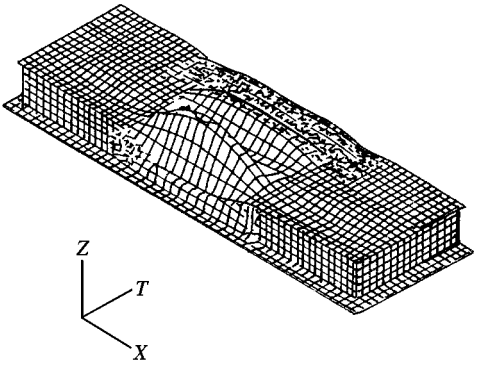

s = 15

Figure 7. Six modes, s = 1, 4, 5, 11, 12, 15, with frequencies respectively 393, 466, 496, 676, 683 Hz of oscillation of the panel, with symmetric boundary conditions.

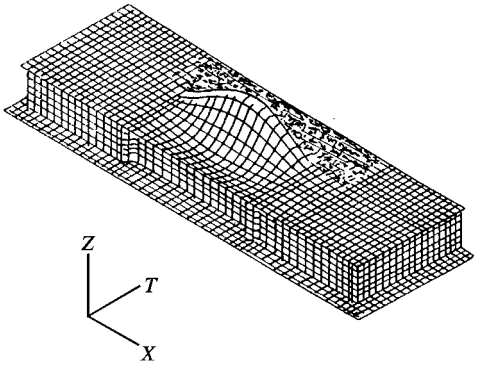

a = 1

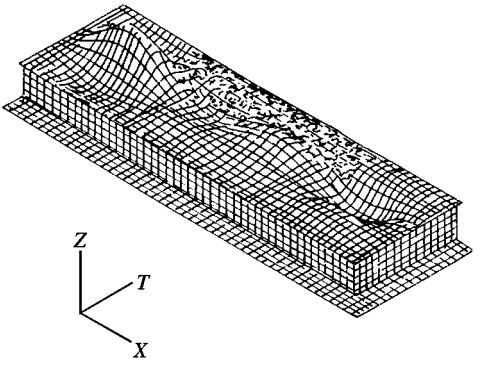

a = 3

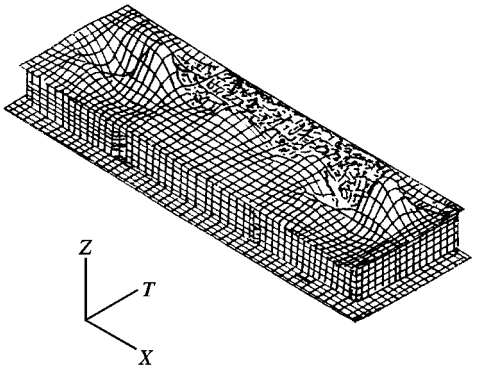

a = 7

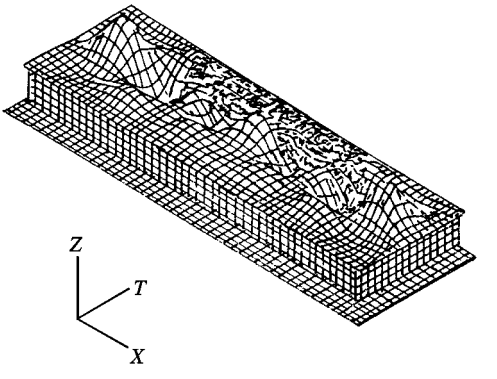

a = 8

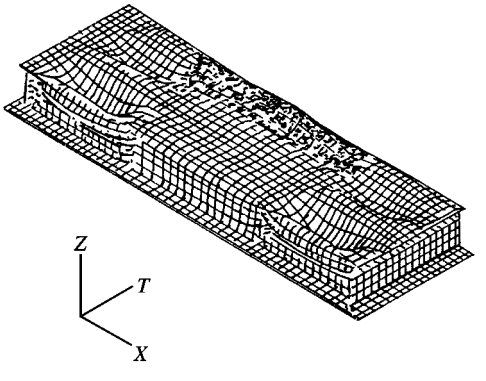

a = 11

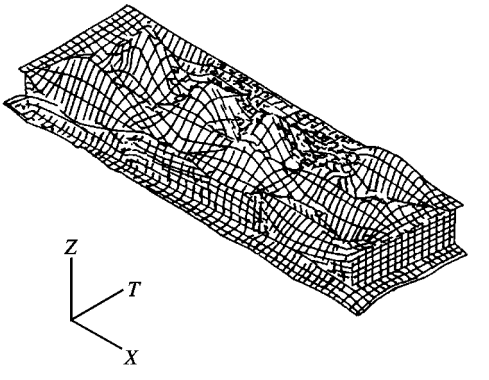

a = 14

Figure 8. Six modes, a = 1, 3, 7, 8, 11, 14, with frequencies respectively 446, 530, 720, 730, 869 and 926 Hz of oscillation of the panel, with skew-symmetric boundary conditions.

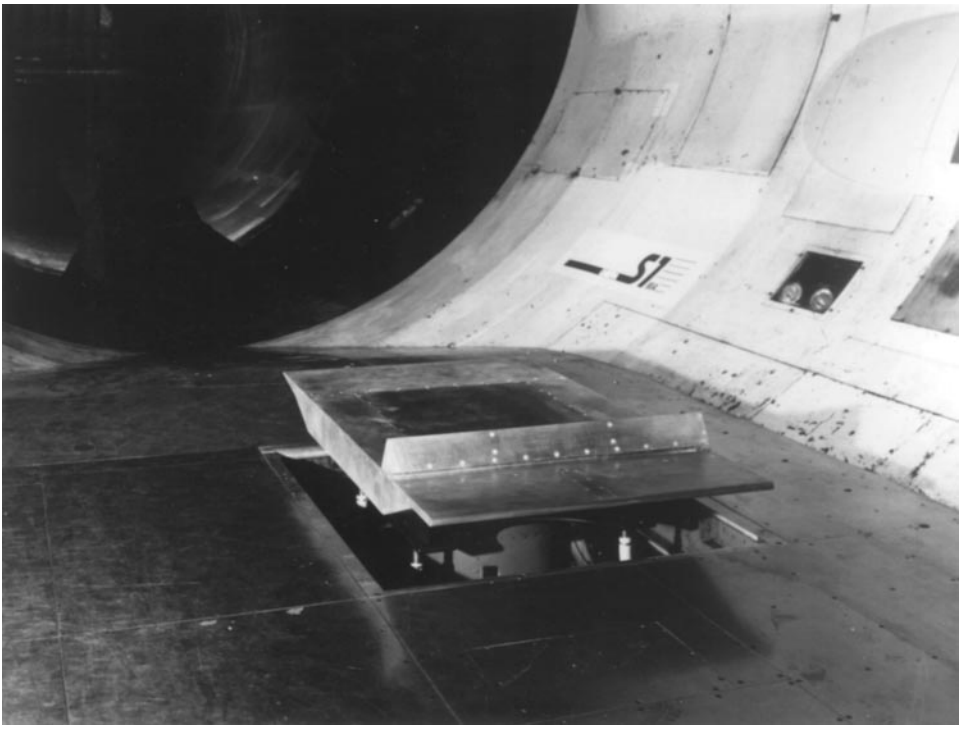

Figure 9. Photo of test set-up, from the upstream position, in the ONERA Modane S1 transonic tunnel, which has an 8 m diameter test-section, showing the flap and test panel, which cause a relatively small blockage, and are elevated from the tunnel wall, to avoid the wall boundary layer and lie in the potential core flow.

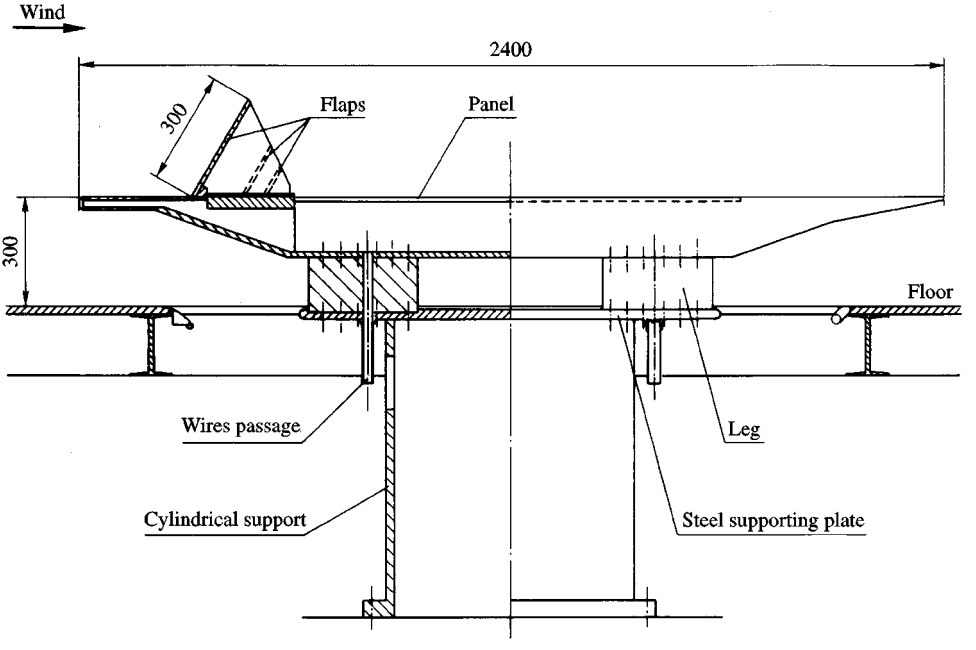

Figure 10. Cross-section of test set-up showing four interchangeable flaps, upstream of the testpanel, the whole being elevated relative to the tunnel wall, by a support structure, through which pass sensor signal wires. Dimensions are in mm.

these phenomena have to be taken into account in the numerical model of the dynamical behaviour or the mechanical system, allowing correct interpretation of the experimental results; numerical simulations of the response spectra of specimen also emphasize the major importance of properly modelling the cross-correlation terms of the input pressure field.

In the present work an aeroelastic model was used, in the sense that the correlation of acoustic pressures was used as an input load for a finite element structural code, as described in Section 3.1. No account was taken of fluid–wall coupling effects in the sense of modifying the input acoustic field due to deflections of the panel. The omission of the back-reaction of the panel on the sound field is a reasonable approximation, and allows the use of standard aeroelastic codes, with an improved load input, calculated from the statistics of sound as indicated in Section 2.

3.3. Geometry of the Flow behind the Flap

Figure 11 presents a sketch of the flow pattern behind the flap, which, as could be expected, shows a recirculation bubble covering most of the test panel. In a real aircraft application, the slot between the flap and the wall, would give rise to a detached recirculation bubble instead. Also shown are the locations of minimum steady pressure associated with the mean flow, and maximum r.m.s. pressure associated with the turbulent perturbations, and the reattachment zone. The location of the recirculation bubble can be seen in the plots of r.m.s. pressure versus longitudinal coordinate (Figure 12), as a bulge, the end of which indicates the start of the reattachment region. Although the largest flap, of height 300 mm and width 1300 mm, would appear to be a relatively "small blockage" for an 8 m diameter wind tunnel, it did in fact lead to a very unsteady wake, which would "hit" the panel, and cause strongly oscillating pressure signals; for this reason, r.m.s. pressure measurements were made for the other three, "not so large" flaps, viz., the results for the tallest, widest flap are shown at the top of Figure 12, with a lower flap at the bottom of Figure 12, and a narrower flap at the top of Figure 13. In all these figures it is clear that the r.m.s. pressure increases with the Mach number of the incident stream; this is shown also at the bottom of Figure 13, where it is seen that the r.m.s. pressure is higher for the higher flaps or those of larger span. Even for the smaller flaps, the blockage effect was sufficient to limit the attainable Mach number to little over $M = 0{\cdot}9$. The recirculating flow in the wind tunnel is not relevant to the present acoustic model, because it is not the cause of the randomness of the sound field; the latter is due to the irregular shape of the wake, which is the essential feature, sketched in Figure 1.

3.4. Location of Strain Gauges and Microphones

Another photo of the wind tunnel set-up, from the top (Figure 14) instead of from the front, shows clearly the location of the test panel relative to the flap. Actually two test assemblies were used in the AWT: (i) one had imbedded 21 strain gauges and six accelerometers (Figure 15), fitted to the text box, for the measurement of structural response, which is one of the sets of data of prime practical interest; and (ii) the other mounted a panel with 40 imbedded microphones (Figure 16), to measure pressure loads, which are important for the understanding of acoustic fatigue, in two ways: (a) by providing the load input to the structural code, for computation of the response; (b) by providing the correlation of loads, for comparison with the theoretical model, and determination of semi-empirical parameters. Note that two microphones were placed outside the test panel, to serve as a reference; of the remaining 38 microphones, 35 were placed on the longitudinal axis or to one side of it, leaving three on the other side, to check for symmetry.

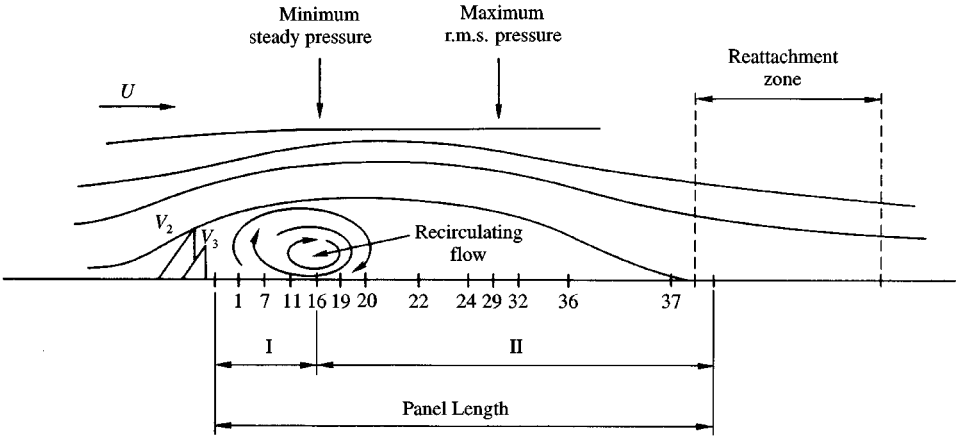

Figure 11. Sketch of the recirculation bubble and reattached flow behind a flap, and the flow deflected over the test panel, showing the points of minimum steady pressure due to the mean flow, and the point of maximum root-mean-square pressure of the fluctuations.

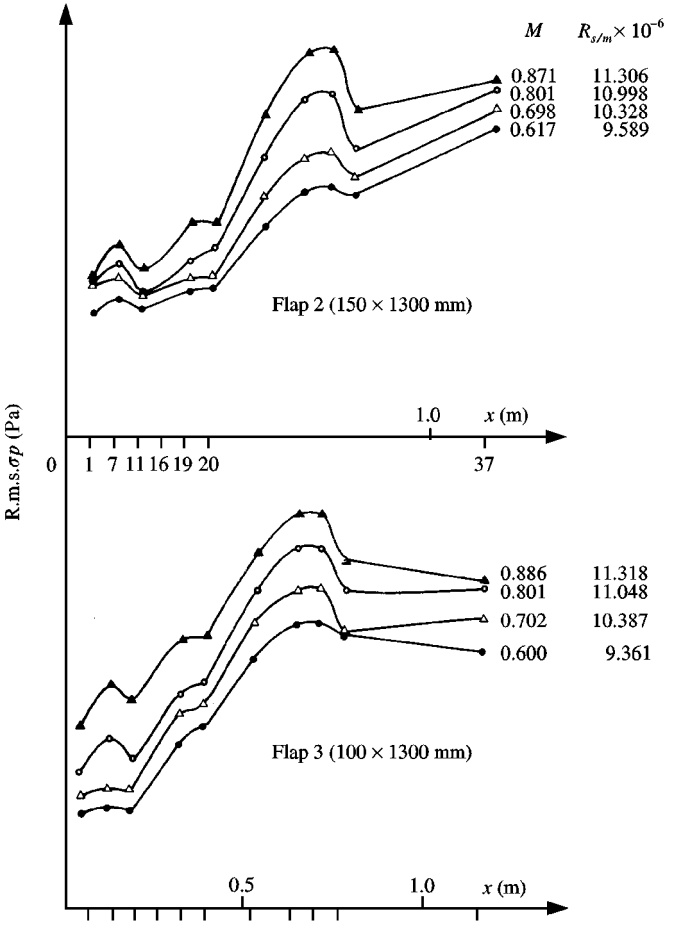

Figure 12. Root-mean-square pressure plotted versus distance along the axis of the test panel, for four values of the Mach number M, and corresponding Reynolds number Re per meter, in the case (top) of a tall and wide flap, and (bottom) a lower flap of the same width.

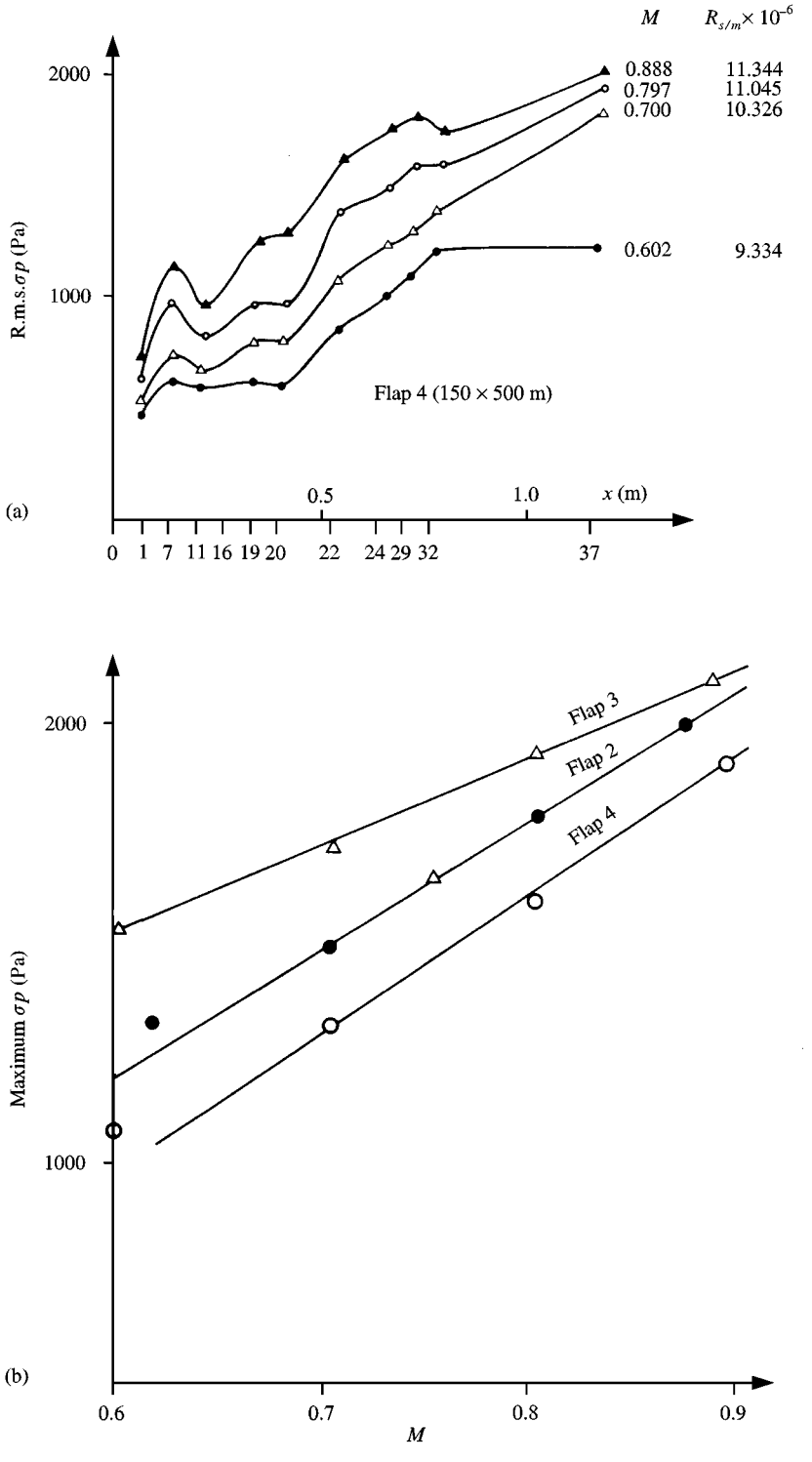

Figure 13. (a) As Figure 12 for a tall and narrow flap. (b) Comparison, for the three preceding flaps, of the r.m.s. pressure as a function of Mach number M, measured at microphone M29 (see Figure 16).

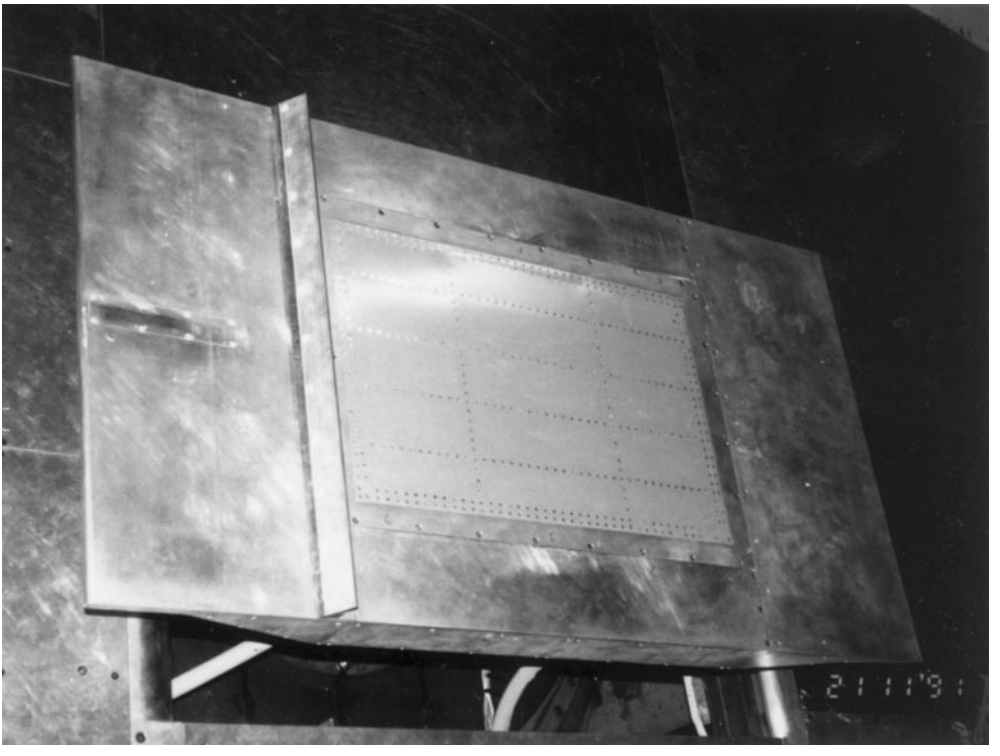

Figure 14. Overhead photo of test set-up, showing the flap and the test panel behind it, and the spacing of the ensemble from the tunnel wall.

Some of the precautions taken, in the installation of the microphones, to ensure that these acted as pressure transducers, relatively unaffected by accelerations, deserve mention. The microphones (1/8 in Brüel & Kjaer) were not exactly flush-mounted. After removing the original grid, they were placed in cylindrical holes crossing the panel, the sensitive membrane being slightly below the surface of the panel. A small thin plane grid, with very small holes, was flush-mounted on the panel, just above that membrane, in order to protect it, and to avoid any surface discountinuity which could cause aerodynamic and/or acoustic perturbations. A precise mounting ensures that the spacing between the membrane and the grid is very small, avoiding any Helmholtz resonator effect in the frequency range of interest. After mounting the sensors on the panel, an acoustic test was performed to check calibrations and transfer functions of the channels, by comparison with the response of an unmodified external sensor which was displaced successively at the immediate vicinity of each sensor. The capacitive-type microphones used have low sensitivity to vibrations; in addition, special attention has been devoted to the local miniaturized electronics, in order to avoid or to minimize any spurious signal due to dynamical excitations. Furthermore accelerometers were placed on the panel during these tests, allowing to focus attention, if necessary, to any special unwanted vibrational event.

3.5. Measured Powder and Cross-Correlation Spectra of Sound

The measured power spectra vary significantly with microphone position. There is broadband noise in the range 0–400 Hz, with a peak at about 100 Hz, more or less marked (Figure 17). The frequency of the peak is Doppler shifted, as the Mach number of the test is varied.

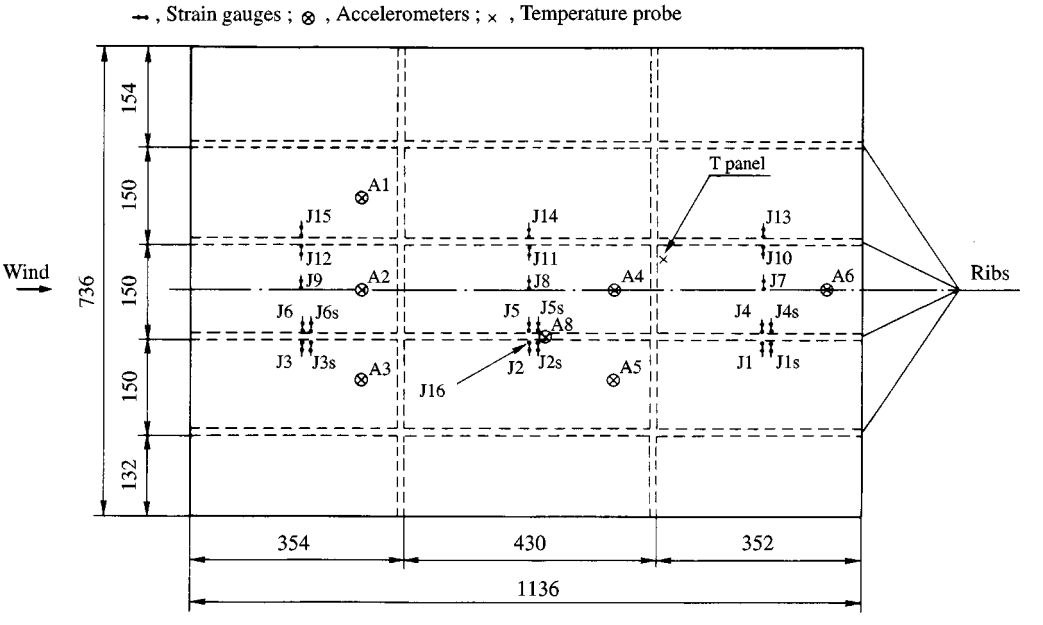

Figure 15. Location of six accelerometers A1–A6, 21 strain ganges J1–J15 and J1s–J6s and one temperature probe, on the test panel. Dimensions in mm.

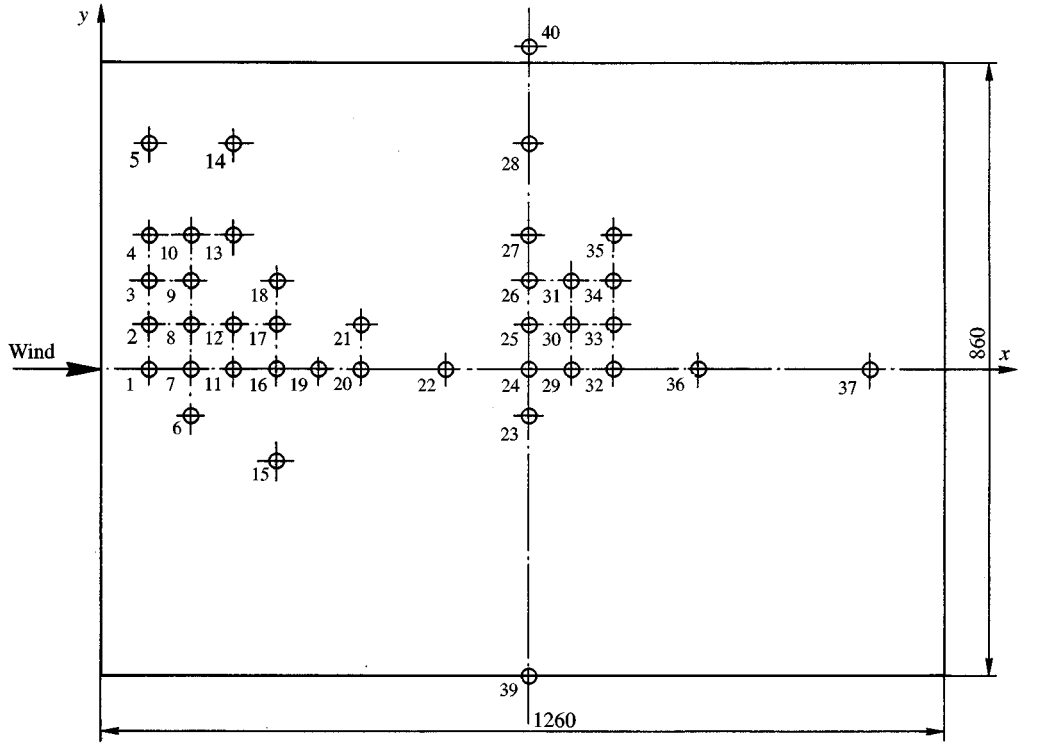

Figure 16. Location of 40 microphones M1–M40, of which two lie outside the test panel for control purposes (M39–M40), and 35 on one-half of the test panel, with three (M6, M15; M23) on the other side, for longitudinal symmetry check. Dimensions in mm.

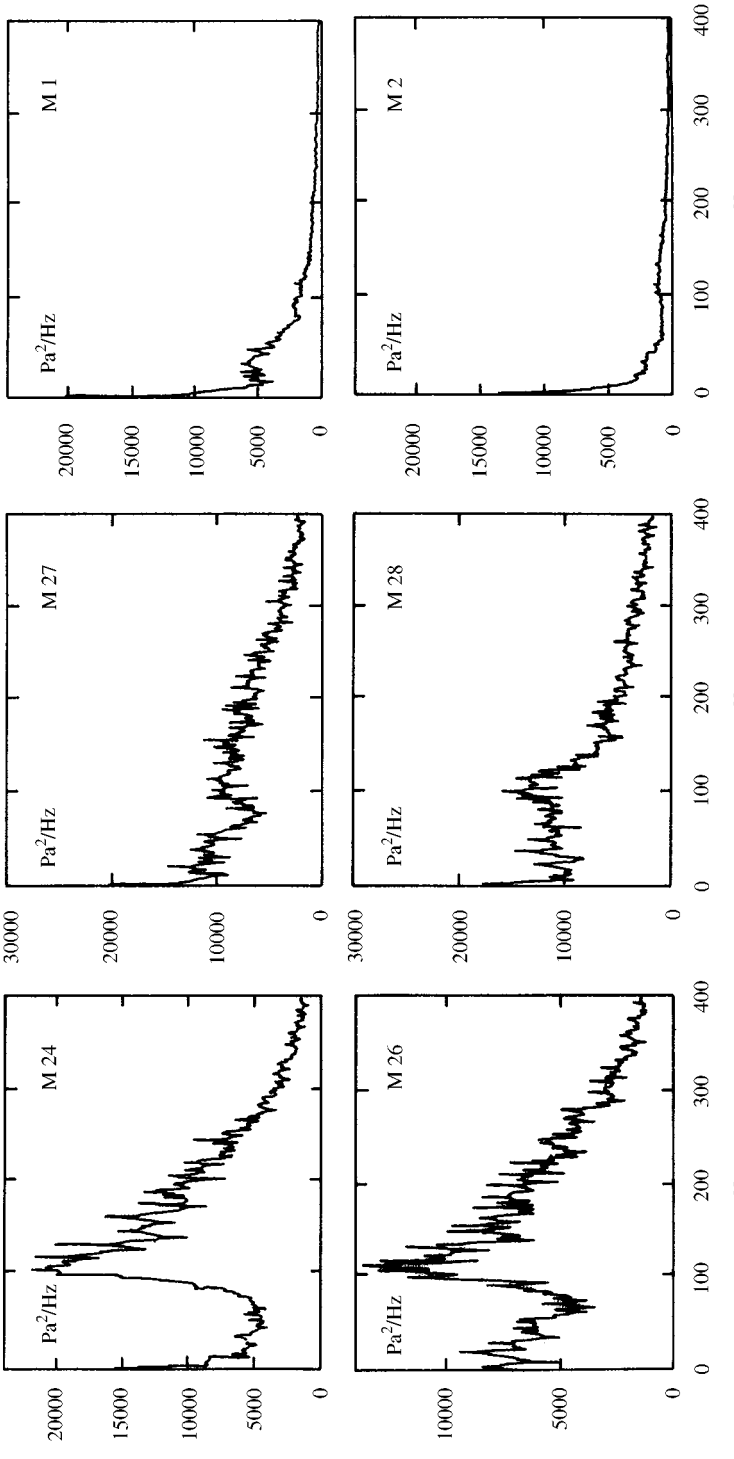

Figure 17. Power spectra at six microphone positions, including examples with (M24, M26) noticeable peak at about 100 Hz, and others (e.g. M28) with a broad spectrum.

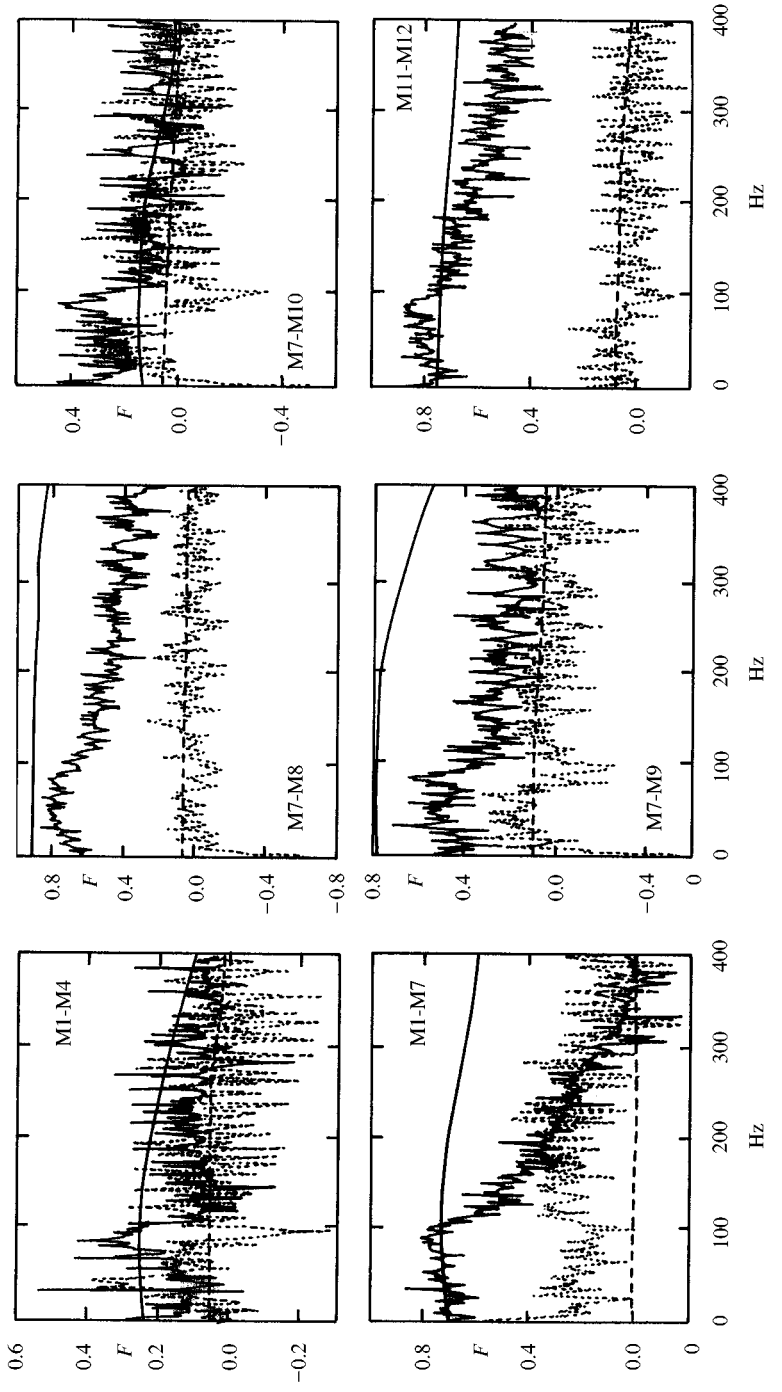

Figure 18. Cross-correlation spectra for six pairs of microphone positions, showing the real part (solid line) and imaginary part (dashed line). The experimental data (jagged) lines is easily distinguished from the theoretical (smooth) curves.

The peak is more marked for microphones like M24 or M26, i.e. near the axis, at some distance from the flap. The power spectral density looks more like a broadband spectrum at other positions, e.g. for microphones M1 or M2 near the axis close to the flap, or for microphones M27-28 off-axis far from the flap. The pressure fluctuations are smaller in absolute value on-axis close to the flap (M1, M2), and increase downstream farther from the flap (M27, M28), in particular close to the axis of the panel (M24, M26).

The number of pairs of microphones, for which cross-correlation spectra can be measured, is quite large ($40 \times 39 : 2 = 780$), and only a very small fraction is shown in Figure 18. It is seen that the imaginary part of the cross-correlation is small in almost every case, and averages about zero; the real part of the cross-correlation is larger, but it rarely exceeds 0·6, even for closely spaced microphones. The correlation is larger for closer microphones (such as M7, M8 or M11, M12), and decays faster at high-frequency for longitudinal than for transversal pairs (e.g. compare M1–7 with M7, M8 and M7–10). This suggests that the correlation length is between one and three microphone grid spacings; also it is larger in the direction transverse to the flow, as should be expected, from the fact that gradients are smaller in this direction. The preceding remarks relate to the estimation of the eight semi-empirical parameters of the theoretical model given by Section 2.9 by comparison with measured power and cross-correlation spectra.

3.6. Eight Semi-Empirical Parameters of the Theoretical Model

The values taken for the parameters in the model are as follows:

(a) double reflection coefficient: $D = 0$; this is equivalent to neglecting multiple scattering, i.e. only the first reflection of sound waves between the structural panel and turbulent wake contributes to random phases and wave interference;

(b) excitation frequency: $\omega_0 = 2\pi \times 100$ Hz; this is the observed main peak in AWT tests;

(c) longitudinal excitation wavenumber: $k_0 = 1{\cdot}11\ \mathrm{m}^{-1}$; use of this value in the formula $k_0 \sim k_x = (\omega_0/c)\cos\theta$, with a sound speed $c = 340\ \mathrm{m\,s}^{-1}$, gives $\theta = 53^\circ$ for the angle of sound waves with the plate;

(d) transverse excitation wavenumber: $K_0 = 0{\cdot}05\ \mathrm{m}^{-1}$; using the formula $K_0 \sim k_y = (\omega_0/c)\cos\varphi$ gives $\varphi = 88^\circ$ for the angle of sound waves with flow;

(e) root mean square phase shift: $\sigma = 2$. Since $\sigma \geq 1$, the effects of random phase shifts are significant;

(f) longitudinal correlation scale: $L = 25$ cm; this should be compared with the fact that in AWT tests the correlation became quite small for distances of more than 20 cm;

(g) transversal correlation scale: $\ell = 50$ cm; this should be larger than the longitudinal one $\ell > L$, because the flow is less disturbed transversely to the flap, than in the flow direction;

(h) correlation time: $T = 0{\cdot}003$ s is of the order $2\pi L/c = 0{\cdot}005$ s, taking the sound speed for the phase speed of interaction.

In conclusion, the values taken for the eight parameters appear to be reasonable, and were in fact not subject to much adjustment.

3.7. Comparison of Experimental, Empirical and Theoretical Response

The panel response, at two of the eight strain gauge positions, is shown respectively in Figures 19 and 20. Each consists of three plots: the "experimental" response (centre), measured by strain gauges imbedded in the test box, in the wind tunnel; the "empirical" or hybrid response (bottom), calculated by the finite element code, using as input the correlation

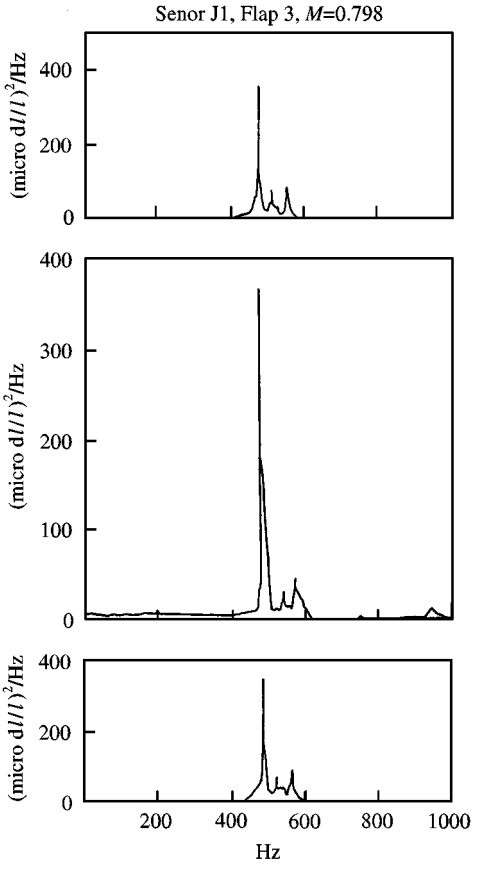

Figure 19. Comparison of panel response at gauge J1: (centre) measured in wind tunnel; (bottom) calculated by Elfini code, using correlation of loads measured in wind tunnel; (top) calculated by Elfini code, using analytical formula for correlation of loads.

of acoustic pressures measured by the microphones, inbedded in the test panel in the wind tunnel; the "theoretical" response (top), again calculated by the finite element code, using as input the correlation of acoustic pressures specified by the analytical formula derived in Section 2.9, with the values of the parameters indicated in Section 3.6, which arise from a comparison with experiment. The designations "experimental", "empirical" and "theoretical" response are not exact, since all three involve experimental data, but they do indicate that experimental input is gradually smaller relative to the computational and theoretical part. There is quite good agreement of the three regarding the panel responses, both for gauge 1 in Figure 19, where there is one dominant peak, and for gauge 2 in Figure 20, where there are several peaks. The good agreement concerns the height (dB level) and location (frequency) of the peaks, their separation in frequency and difference in level, and the shape of the remaining spectrum. Note that the two gauges were at very different locations as shown in Figure 15, viz. J1 is far from the flap and J2 closer to it. The latter location gave the more complex, multi-modal response spectrum.

3.8. Comparison of Measured and Calculated Correlation of Loads

The good agreement of the three response curves in Figures 19 and 20, shows that; (i) the finite element code can successfully predict acoustic fatigue response, if the correlation of

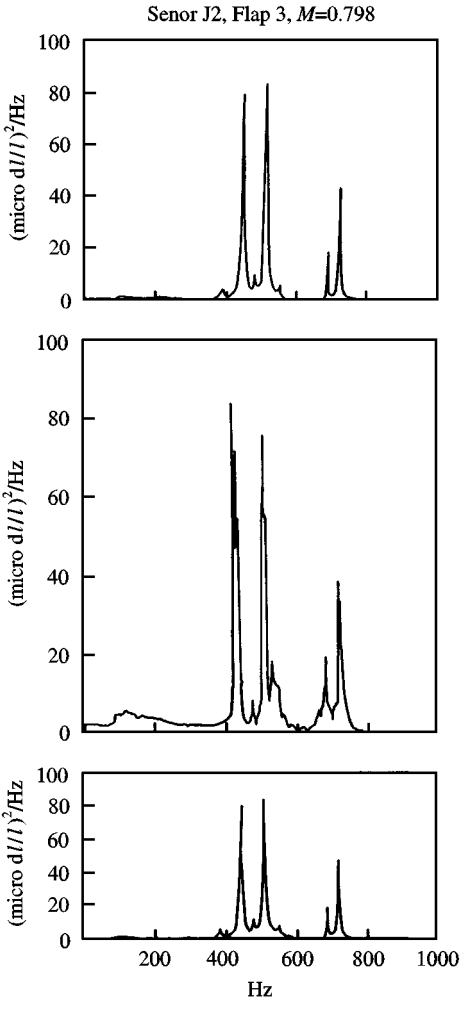

Figure 20. As in Figure 19, at gauge J2, where response is multi-modal.

loads is accurately provided as an input; and (ii) the correlation of acoustic pressures measured by microphones can be replaced, by the analytical formula derived in Section 2.8, with semi-empirical parameters indicated in Section 3.6, and gives a comparable response. These two conclusions are important, because they show that, although acoustic fatigue has been treated almost exclusively by empirical methods in the past, in fact: (a) it is not a "new" structural phenomenon, but "merely" a matter of specification of loads; (b) the most "difficult" feature of the loads, which is their correlation, can be modelled theoretically. Going further, and comparing directly the loads, it is clear from Figure 18 that the agreement of measured and theoretical correlations of acoustic pressures, is much less satisfactory than for panel responses (Figures 19 and 20). The measured loads are the jagged lines and the theoretical correlations the smooth curves; the solid lines refer to the real part of the correlation coefficient and the dotted lines to the imaginary part. It should be noted that the values of the semi-empirical parameters used in the analytical formula derived in Section 2.9, were obtained as indicated in Section 3.6, and with little adjustment gave satisfactory panel responses; thus there was little to do to optimize the eight parameters, to improve the agreement in Figure 18, e.g. multiple scattering was not considered at all.

Nevertheless, the fact remains that the good agreement of panel response was not undermined by the poorer fit of loads; one explanation may be that the analytical prediction and experimental measurement are in better agreement over the range of frequencies where the panel responses are concentrated. Another, possibly more important point, is that the panel response depends on the correlation of pressure loads at many pairs of points, and is not too sensitive to local discrepancies; an adequate global representation of random loads and correlations is what matters for satisfactory modelling of acoustic fatigue.

3.9. Comparisons of Tests in PWTs and AWTs

One can take further the argument that the panel response depends on many pairs of correlation of loads, and thus may not be much affected by a local discrepancy, and depends more on having the right order-of-magnitude in most combinations. One could conceivably stretch the last argument, in a skeptical way, to argue that the implication might be that panel response is relatively insensitive to the correlation of loads. This conjecture is quite false, as can be shown both by using experimental data or results of finite element code. The rather strong sensitivity of the panel response to the correlation of loads is demonstrated in Figure 21, where the finite element calculation (centre) is compared with measurements at

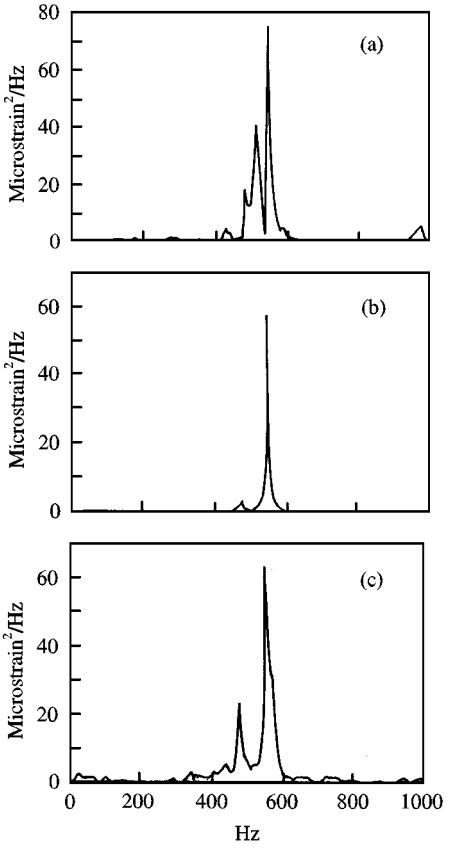

Figure 21. Comparison of response at same gauge J1 as for Figure 19, but: (a) measured at the British Aerospace Filton progressive wave tube; (b) calculated by Elfini code with unit correlation for loads; (c) measured at the IABG Ottobrunn progressive wave tube.

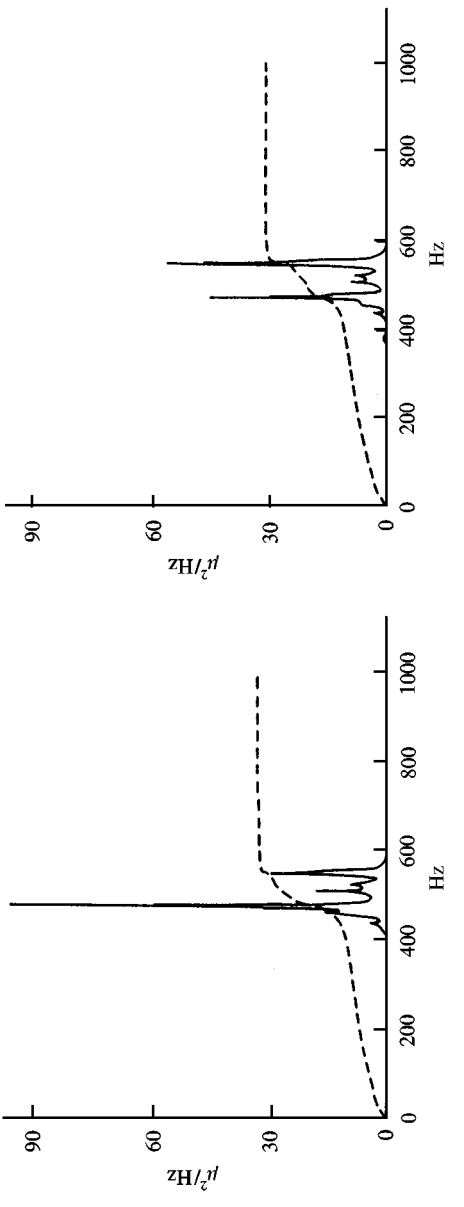

Figure 22. Calculation by Elfini code, of panel response at gauge J1, for four uniform values 0.2, 0.4, 0.6 and 0.8 of correlation of loads, showing how the level of excitation of different modes varies.

two progressive wave tubes (PWTs), at IABG in Ottobrunn (top) in Germany and British Aerospace at Filton (bottom) in Wales. The data refer to the same gauge 1, and show that: (i) the results of the finite element code, which had modelled well the AWT (Aerocoustic Wind Tunnel) experiments, disagree with PWT tests; and (ii) the test results at the two distinct PWTs are also in disagreement, but less so. The explanation may be: (i) that the correlation of loads is dominated by reflections from the side walls and convection by the mean flow in AWTs, and thus is quite different from PWTs, where it is dominated by reflecting surfaces in all directions; and (ii) since the eigenvalues and eigenfunctions of the standing modes, depend on the geometry of the PWT, the results in PWT with different geometries may be distinct. In Figure 21, the response in PWTs differs from that in AWTs, in the number of peaks, their absolute and relative magnitude in dB, and frequency at which they occur. All this may be just a consequence of one effect, namely, a different correlation of loads. This is shown clearly in Figure 22, where the panel response is calculated for four values of the correlation of loads (from 0·2 to 0·8 in jumps 0·2), each assumed uniform over the panel; as the correlation increases, different modes become dominant, e.g. a high (low) correlation is more effective at exciting symmetric (skew-symmetric) modes.

4. CONCLUSION

Although the panel response in the AWT superficially looks like a structural response function, it is not, as can be seen by comparing with the response to white noise excitation over the frequency range considered. White noise excitation corresponds to a unit correlation of loads (see Figure 22 for the highest correlation 0·8 not far from 1·0), in which case the response is different from that measured in the AWT (Figure 19). A uniform correlation coefficient, for values decreasing below unity (Figure 22), shows different responses, but still not matching that measured in the AWT. This is not surprising, since the measured correlation of acoustic loads (Figure 18), shows nonconstant correlations, which strongly depend on the particular pair of microphones selected. There is thus both experimental evidence that the correlation of acoustic loads is not a simple function, and theoretical evidence that a simple correlation function cannot reproduce the structural response found in the AWT. This observation may explain why aeroacoustic fatigue has been difficult to model in the past, and justifies the effort put in the present paper to account for what may be the critical part of the theory: a careful prediction of the correlation of acoustic loads, which, as the preceding remarks might suggest, is not a simple function of separation. The theoretical correlation function used in the computations was in fact simplified, to the leading term of the series expansion derived in Section 2. Although the theoretical correlation function did not match closely the measured one (Figure 18) at most pairs of microphones, the structural response calculated using either of them was similar (Figures 19 and 20). This suggests that the structural response depends on the correlation of acoustic loads over many pairs of points and a plausible physical and statistical description, rather than a precise fit for every pair, is sufficient for a satisfactory model.

The acoustic fatigue is traditionally addressed by purely empirical methods, based on testing in PWTs. The present work has reported on research on acoustic fatigue using both PWTs and AWTs. The latter are less practical as a test facility, but more representative of real flight conditions. Thus the conclusions should address three points, namely, the results of acoustic fatigue tests in AWTs and PWTs and how to possibly bridge the gap between the two. Acoustic fatigue tests in an AWT are an excellent approach to improving the understanding of the phenomenon. The first tests of this kind, have led to two important sets of conclusions. The first is that finite-element code, of the kind used for a wide variety of aeroelastic problems, can also successfully model acoustic fatigue; this shows that acoustic

fatigue is not a physically "new" structural phenomenon, but rather the effect of a complex ensemble of random, correlated loads. The determination of these loads by wind tunnel tests is a powerful research tool, but also a costly and complex one; the ability of an analytical formula to do just as well, for panel response calculations, is a welcome alternative; it also shows that acoustic fatigue is not beyond the reach of mathematical modelling, even in a relatively complex case. The remaining limitation is that the parameters in the theoretical formula still need to be adjusted by comparison with wind tunnel experiments; an alternative, would be to use *a priori* estimates of the parameters, and to fit them by comparing computed and measured panel responses.

Bearing in mind that acoustic fatigue has escaped successful analytic modelling for so long, it may be appropriate to conclude by reviewing what are, and what are not, the essential physical processes underlying the phenomenon. In the experiments which were successfully modelled, the flow configuration was relatively complex, viz., behind the flap there were at least the following flow features: (i) a recirculation bubble; (ii) distributed turbulence; and (iii) a wake which was both irregular and turbulent. It does not follow that all of the flow features are of equal significance to the acoustic problem: (i) propagation of sound through the recirculation bubble, produces deterministic phase shifts, and does not lead to random interference effects; (ii) since the wavelength is large compared to the scales of turbulence, the phase shifts due to local random velocities cannot cause significant interference; and (iii) this leaves the irregular wake, whose thickness is small on a wavelength scale, as the main cause for random phase shifts, by acting as a rough partial reflector.

ACKNOWLEDGEMENTS

The tests in PWTs were performed by Dr G. Bayerdorfer at IABG in Ottobrunn, and Dr P. Green at British Aerospace in Preston. The authors are grateful for the remarks of E. Garrigues, at Dassault Aviation. It goes without saying that the Coordinator of the Acoufat project, D. Tougard at DA, also contributed in many ways to the present work.

References

Abramowitz, M. & Stegun, I. 1965 *Handbook of Mathematical Functions.* New York: Dover.

Beckmann, A. & Spizzichino, P. 1963 *Scattering of Electromagnetic Waves from Rough Surfaces.* New York: McGraw-Hill.

Brekhovskikh, L. M. 1980 *Waves in Layered Media.* Academic Press: London.

Campos, L. M. B. C. 1978a On the spectral broadening of sound by turbulent shear layers. Part I: transmission of sound through turbulent shear layers. *Journal of Fluid Mechanics* **89,** 723–749.

Campos, L. M. B. C. 1978b On the spectral broadening of sound by turbulent shear layers. Part II: Spectral broadening of experimental and aircraft noise. *Journal of Fluid Mechanics* **89,** 751–783.

Campos, L. M. B. C. 1983 Modern trends on research on waves in fluids. Part I: acoustics of turbulent and inhomogeneous flows. *Partugaliae Physica* **14,** 121–143.

Campos, L. M. B. C. 1984 Sur la propagation due son dans les écoulents non-uniformes et non-stationaires. *Revue d'Acoustique* **67,** 217–233.

Campos, L. M. B. C. 1986 On waves in gases. Part I: acoustics of jets, turbulence and ducts. *Reviews of Modern Physics* **58,** 117–182.

Campos, L. M. B. C. 1989 On a generalized Mittag–Leffler theorem and implicit differintegration. *SIAM Journal of Mathematical Analysis* **20,** 454–567.

Campos, L. M. B. C. 1992 Effects on acoustic fatigue loads of multiple reflections between a plate and a turbulent wake. *Acustica* **76,** 109–117.

Campos, L. M. B. C. 1996 On the correlation of acoustic pressures induced by a turbulent wake on a nearby wall. *Acustica* **82,** 9–17.

Campos, L. M. B. C. 1997 On the spectra of aerodynamic noise and aeroacoustic fatigue. *Progress in Aerospace Sciences* **33,** 353–389.

Courant, R. & Hilbert, D. 1953 *Methods of Mathematical Physics.* New York: Interscience.

Ho, C. M. & Kovasznay, L. S. G. 1976a Propagation of a coherent acoustic pulse through a turbulent shear flow. *Journal of the Acoustical Society of America* **60,** 40–45.

Ho, C. M. & Kovasznay, L. S. G. 1976b Acoustical shadowgraph. *Physics of Fluids* **19,** 1118–1123.

Howe, M. S. 1976 On the attenuation of sound by randomly irregular impedance layer. *Proceedings of the Royal Society* (London) **A347,** 513–535.

Ishimaru, A. 1978 *Wave Propagation and Scattering in Random Media*, Volumes 1 and 2. London: Academic Press.

Khinchin, S. I. 1948 *Mathematical Foundations of Statistical Mechanics.* New York: Dover.

Lindeberg, G. J. W. 1922 Eine neue Erleitung des Exponentialgezetzes in der Wahrscheinlichtkeitsrechnung. *Mathematik Zeitschsift* **15,** 211–225.

Nicot, Ph. & Petiau, C. 1987 Tendences actuelles de l'analyse aeroelastique des avions militaires. *L'Aeronautique et L'Astronautique* **122,** 10–25.

Ogilvy, J. A. 1991 *Theory of Wave Scattering from Random Rough Surfaces.* Bristol: Institute of Physics Publishing.

Rayleigh, J. W. S. 1945 *Theory of Sound.* New York: Dover.

Schmidt, D. W. & Tillman, P. M. 1970 Experimental study of sound phase fluctuations caused by turbulent wakes. *Journal of the Acoustical Society of America* **47,** 1310–1324.

Tougard, D. 1993 Brite-Euram Programme: Acoufat-acoustic fatigue and related damage tolerance of advanced composite and metallic structures, AGARD SMP Symposium on *Impact of Acoustic Loads on Aircraft Structures*; *in AGARO CP*-549, *pp.* 16–1 *to* 16–12. Lillehammer, Norway.

Tougard, D. 1995 Acoustic fatigue and related damage of advanced composite structures. In *Advances in Acoustics Technology* (ed. J. M. Martin-Hernandez). Chichester: Wiley.

Uscinski, B. J. 1977 *Elements of Wave Propagation in Random Media.* New York: McGraw-Hill.

von Mises, R. 1964 *Mathematical Theory of Probability and Statistics.* New York: Academic Press.